AD-A258 815

AFIT/GE/ENP/92D-01

DTIC
ELECTE
S JAN 6 1993
C D

Design and Characterization of Optically Pumped
Vertical Cavity Surface Emitting Lasers

THESIS

Richard J. Bagnell
Captain

AFIT/GE/ENP/92D-01

93 1 04 026

AFIT/GE/ENP/92D-01

Design and Characterization of Optically Pumped Vertical Cavity Surface
Emitting Lasers

THESIS

Presented to the Faculty of the School of Engineering

of the Air Force Institute of Technology

Air University

In Partial Fulfillment of the

Requirements for the Degree of

Master of Science in Electrical Engineering

Richard J. Bagnell, B.A., B.S.E.E.

Captain

December, 1992

Accession For

NTIS	GRA&I	☑
DTIC TAB		☐
Unannounced		☐
Justification		

By
Distribution/

Availability Codes

| Dist | Avail and/or Special |

A-1

Preface

The goal of this research was to establish a means of designing and measuring Vertical Cavity Surface Emitting Lasers (VCSELs). The design described and methods of characterization used herein constitute the first capability to build and measure these devices at the Air Force Institute of Technology, and Wright Patterson AFB. The capabilities for fabrication, and tools for more sophisticated measurement practices, will build on the lessons learned from this effort. I want to express sincere thanks to several people and organizations for their help in this research. I'd like to thank my thesis advisor, Capt Jeff Grantham, for his willingness to share his expertise in this area; especially the lab configurations, where I had very little experience. His first hand knowledge of VCSEL experimentation was irreplaceable and allowed the accomplishment of twice my expectations. Mr Rick Patton deserves my appreciation also. His technical expertise and ability to get what the experiment needed on a moment's notice was remarkable. I'd also like to thank Mr. Greg Smith for his help with the dye laser, the attenuator, and the Ti-Sapphire system, which saved me days at least (weeks, ... maybe).

Thanks also to Wright Labs/ERL, who grew the back mirror perfectly, RADC/-OCPA, who sponsored the work and provided funds for several pieces of critical equipment, and the University of Arizona, who provided several VCSEL wafer samples and growth information.

Finally, I thank my wife Yvonne and children, J.C., Marcus, and Kristina, who provided the love and support that was necessary to carry me through this effort. Although I know the kids were good, Yvonne still had her hands full. I owe her tremendously. You can start your vacation tomorrow, Yvonne.

Richard J. Bagnell

ii

Table of Contents

List of Figures

.

.

ix

Abstract

Vertical Cavity Surface Emitting Lasers (VCSELs) are a form of semiconductor laser which have their cavity oriented orthogonally to the plane of the wafer. This orientation necessitates short cavities, requiring highly reflective mirrors and a relatively high gain/loss ratio in the active region. The resultant superior exit beam characteristics (circular beam output, low threshold), the capability of the structure to be arrayed, and the tight packing density of the finished lasers, provide strong motivation for pursuing the growth of these structures. This thesis details the design of an optically pumped InGaAs multiple quantum well periodic gain structure VCSEL with a 950 nm lasing wavelength. These growths are to be a first attempt at VCSEL construction, so part of this study included verification of the quality of the back mirror growth to determine if it met the design specifications. The research included construction of a laboratory configuration to measure spectral reflectivity and optically pump the finished VCSELs. This provided a means to guide the growers in the fabrication of these devices, and validate lasing properties in the finished devices. The VCSELs were characterized by spectral reflectivity, output beam polarization, mode, lasing wavelength, and optimal pump wavelength. Analysis of the characteristics for several VCSELs obtained from the University of Arizona, and the back mirror grown locally, illustrated the ability to use measured data and theoretical spectral reflectivity calculations to determine the quality of the growths. This method can be used to provide a guide for subsequent VCSEL growths. The reflectivity analysis can determine if the growth parameters have been roughly achieved, but do not guarantee the quality and quantity of lasers on the wafer.

Design and Characterization of Optically Pumped Vertical Cavity Surface Emitting Lasers

I. Introduction

This thesis investigates the design and characterization of optically pumped vertical cavity surface emitting lasers. Research into the design of Surface Emitting Laser (SEL) structures has increased dramatically over the past decade. Initially, this type of design was explored to take advantage of the ability to array the SEL in two dimensions [29], allowing tighter packaging of individually-addressed lasers. Vertical Cavity SEL (VCSEL) designs have been aggressively pursued over the past few years because VCSELs have additional inherent advantages. The VCSEL design exhibits better exit beam quality, is of smaller size, and can entail less complex fabrication. These advantages, coupled with the increasingly widespread access to the necessary fabrication technology to make VCSELs (e.g. Molecular Beam Epitaxy (MBE) and Metal-Organic Chemical Vapor Deposition (MOCVD)) motivated the research in this area over the past ten years. VCSELs are an emerging technology, and may provide dramatic improvements in surface emitting thresholds, power output, and optical channel capacity. To now, commercial applications have driven the research. Military applications in higher output power, beam steering, and heads-up displays, for example, may proceed more briskly with the development of an in-house VCSEL fabrication and test capability. This research provides an initial design and characterization capability.

1.1 Background

The typical VCSEL consists, as with other semiconductor lasers, of a semiconductor gain medium (III - V compound) and a set of mirrors. The design of both the gain medium and the mirrors is critical to output performance. Although it is an integrated structure, the VCSEL can be thought of as having three regions (see Figure 1.1). The top and bottom

regions are Distributed Bragg Reflector (DBR) mirrors, and the middle region is the laser cavity.
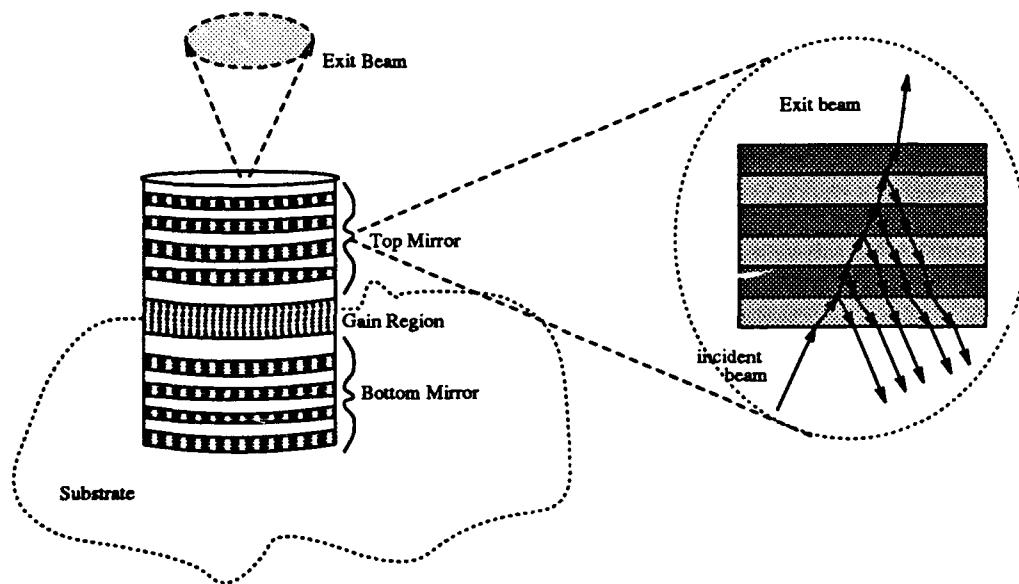
Figure 1.1. Vertical Cavity Surface Emitting Laser (VCSEL Geometry)

1.1.1 **DBR Mirrors** The advantage of MBE/MOCVD lay down technology is that these methods each can deposit the mirrors and cavity in one uninterrupted process. This is done by forming the mirrors of multi-layer films (see Figure 1.1 inset). The change of refractive index between layers in the multi-layered stack results in a reflected and transmitted component of the incident light at each interface. The multiple reflections and transmissions in the stack can be engineered to selectively transmit or reflect at desired frequency bands [26]. MacLeod outlines criteria governing the reflectances at each interface:

- The intensity reflectance of light at each interface is given by $[(1 - \rho) / (1 + \rho)]^2$ where ρ is the ratio of the refractive indices of the media on each side of the interface.

- There is a phase shift of 180° when the reflectance is in a medium with a lower refractive index than the adjoining medium. The phase shift is 0° for higher- to lower-index transitions.

- The components of light from the multiple reflections in the stack constructively interfere (add) if the relative phase shift is a multiple of 360° and destructively interfere if the relative phase shift is an odd multiple of 180°.

In the DBR, high reflectance is accomplished by making the layers in the stack precisely one-quarter wavelength ($\lambda/4$) thick for the wavelength to be reflected. The light incident at one interface will traverse this thickness and partially reflect off the next interface, and each succeeding interface. The layers are $\lambda/4$ thick, which produces a π phase shift between successive reflections, and there is an added π phase shift at the lower-to higher-index interfaces; as these components return, they will be in-phase and constructively interfere, producing an overall high reflectance at the wavelength the stack is designed for. Wavelengths of incident light which are significantly longer or shorter than this wavelength will have less dramatic reflectance from the stack.

The DBR mirror design produces highly reflective mirrors. We must consider more than just the reflectance, however, for the mirrors to form a good semiconductor laser mirror. The refractive index, absorption coefficient, and lattice matching considerations all impact the choice of mirror materials. These factors will be addressed to a greater depth in later sections.

1.1.2 **VCSEL Cavity** The cavity for the VCSEL contains the gain medium, where the population inversion of carriers allows stimulated emission to produce the exiting beam. This cavity can be completely composed of active material, but it is now more common to see a cavity which uses a periodic gain structure. That is, the active regions of the cavity reside only at the places in the cavity where the electric field standing wave will form a maximum (see figure 1.2). These active regions can be formed of bulk material or of multiple quantum wells, with barriers interspersed, to take advantage of quantum effects. The choice of materials in this region is affected by the desired gain for the region, the absorption of the spacer and the active regions, the lasing wavelength, and lattice matching considerations.
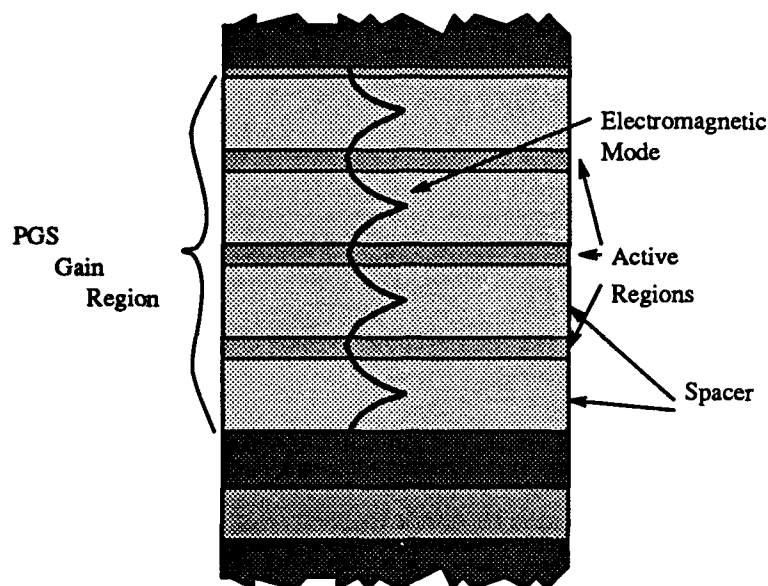
Figure 1.2. Periodic Gain Structure (PGS) Cavity

1.1.3 VCSEL Characteristics

Reflectivity Together, the cavity and the mirrors form an integrated Fabry-Perot etalon. In the VCSEL, the Fabry-Perot etalon structure provides an effective energy storage mechanism. The spectral reflectivity curve is characterized by regions with high transmittance and reflectance, and optically pumped VCSEL structures exploit these areas of the curve.

A typical curve for a bulk GaAs VCSEL illustrates the Fabry-Perot effect in Figure 1.3. The resonance at 880 nm is flanked by highly reflective regions (~ 99.9 %). This high reflectivity is achieved with less than 25 pairs of AlAs/GaAs $\lambda/4$ layers in the top and bottom mirror stacks. In optical pumping, another laser is used to generate carriers in the VCSEL. Thus, the mirrors must be highly transmissive at the "pumping" wavelength to allow the laser light to reach the gain medium. For this reason, carriers are injected at a wavelength (the pump wavelength) near the edge of the highly reflective stop band, where the structure is highly transmissive. In this case, a likely pump wavelength would

1-4

be near 820 nm. The curve below was constructed using the transmission matrix approach discussed in Chapter II and the FORTRAN programs included in Appendix A.
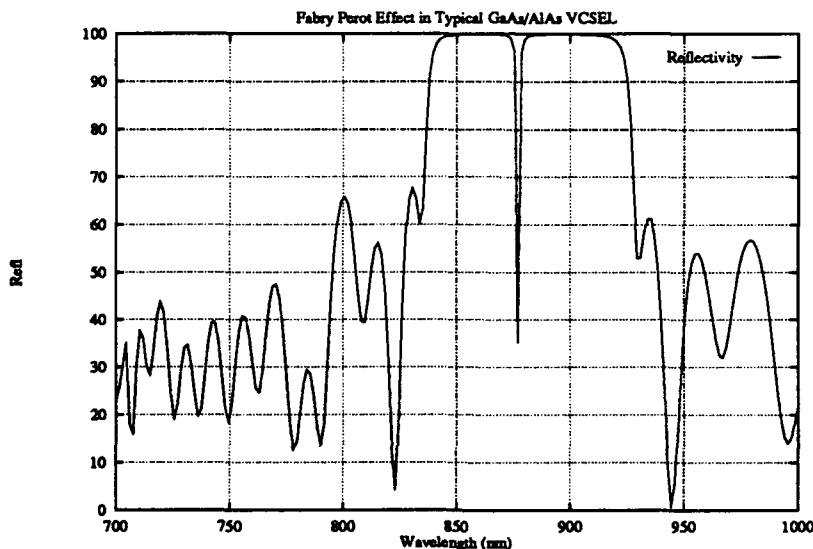
Figure 1.3. Fabry Perot Effect in Typical VCSEL

The reflectivity curve illustrated in Figure 1.3 is dependent on the uniformity of the layers in the mirrors, the cavity, and the substrate, and the index of refraction of the materials in these regions. The ability of the manufacturer of the VCSEL to control these parameters will determine how closely the finished product meets the reflectivity curve.

Polarization Strain in the interfaces between layers in the active regions and in the mirrors can affect the output characteristics of the VCSEL. In InGaAs quantum well active regions, strain can produce polarized output [6]. Compressive strain tends to produce TE polarization, while tensile strain favors TM polarization [10]. For active regions constructed of $Al_x Ga_{1-x} As$ layers, the close lattice match in these ternaries over the range of x concentrations provides minimal strain. Polarization measurements for bulk GaAs active region VCSELs indicate no favored direction in the linear polarizations [21].

Mode Selection Single longitudinal mode operation is a highly valued inherent feature of VCSELs, even though typical in-plane semiconductor lasers can have

natural mode spacings on the order of hundreds of GHz. The small cavity size ($\sim 3\mu m$) makes the Fabry-Perot structure highly mode selective. The actual mode spacing is difficult to calculate, since the DBR mirrors have penetration depths which contribute to an *effective* cavity length which can be much greater than the designed cavity length [20]. The effective cavity length, however, is normally small enough to preclude higher order longitudinal modes in VCSEL structure.

Higher order transverse modes have been noted in several studies [17]. Jewell noted that higher pump intensities and slightly misaligned input beams were required to excite these modes [21]. The transverse mode order VCSELs exhibit depends on the transverse dimensions of the structure, larger transverse dimensions supporting higher order transverse modes [8].

Power The power from theses devices depends primarily on the cooling efficiency and the power efficiency of the geometry. Output power is low in comparison to other types of semiconductor lasers, due to the small geometries involved, which limit the gain volume and provide heat dissipation problems [19]. Pulsed output power has been reported up to .5 W and continuous wave (CW) power above 9 mW [9].

1.2 Problem Statement

This thesis examines the design techniques for building VCSELs, and the characterization of these designs via surface reflectivity, output polarization, frequency, and beam quality.

1.3 Scope

The scope of the effort was to design optically pumped VCSELs, and develop a laboratory capability to guide the fabrication, check quality, demonstrate lasing in the final product, and measure completed VCSEL output beam characteristics and spectral reflectivity. The design considerations examined for this thesis can be applied to produce optically or electrically pumped surface emitters. This thesis purposely focuses on the

optically pumped structures, as the means of producing VCSELs for this effort was limited to optically pumped devices.

1.4 Approach/Methodology

This research had two ends to achieve; the design of sample vertical cavity surface emitters; and to establish a means to characterize them via direct laboratory measurement.

The design part involved building structures to be optically measured. These structures were, basically, prospective parts of a finished VCSEL design. The initial effort was segmented to provide a way to evaluate the growth capabilities of the available MBE system without having to grow entire VCSELs.

Most current designs use distributed Bragg reflector mirrors made of $Al_xGa_{1-x}As$, the high index layers using a low x concentration, and the low index layers using a high x concentration. AlAs/GaAs is a conventional choice for the DBR mirrors for InGaAs lasers, and was chosen because: it would provide a predictable means of determining fabrication quality; the MBE capability available to us was ready to produce this combination without modification; and, successful VCSELs have been grown using this material before [17].

The back mirror was measured to see if it exhibited an adequate match to the desired spectral reflectivity curve. Once the back mirror design was complete, the full VCSEL structure was submitted for fabrication. The gain medium used a periodic gain structure with multiple quantum wells at the peaks of the standing wave electromagnetic mode in the cavity.

The characterization phase involved constructing a laboratory bench configuration to provide a means to measure reflectivity, polarization, lasing wavelength, and beam cross section. The laboratory configuration is discussed in Chapter IV.

1.5 Sequence of Presentation

Chapter II introduces the theory used to design the structures measured for this thesis. The VCSEL and back mirror designs produced by this effort and options for electrical stimulation and other improvements is contained in Chapter III. Chapter IV

provides details on the laboratory configuration used to measure the growth structures. Chapter V details the results of the testing, and Chapter VI summarizes the findings and recommendations.

II. Theory

Building a vertical cavity surface emitting laser follows the design steps for larger conventional lasers. The scale and orientation of the VCSEL cavity produce the design challenge. The first VCSELs were built in the early 1970's [29]. The initial structures involved three distinct regions, the top and bottom mirrors and the gain region. The application of MBE and MOCVD to the process, though, has removed most of the anxiety over the transition between the cavity and the mirrors. The result is a one-step growth which produces an integrated mirror/cavity Fabry-Perot etalon. This section discusses the initial design considerations involved. This order of presentation elaborates on the design choices used in building the InGaAs quantum well VCSELs for this effort, but is readily adaptable to bulk active medium designs.

2.1 Efficient Vertical Cavity Lasers

Although the primary concern in growing the samples for this effort was not efficiency, the ability to incorporate efficient designs in early VCSELs will benefit later designs. Not all applications for VCSELs may require the enhanced efficiency these features bring; but a review of them provides a clearer insight to the design options available.

The goal is to minimize the threshold current density, J_{th} ; the minimum current density required for lasing to occur. J_{th} may be expressed in terms of the nominal current density, the active region thickness, and the internal quantum efficiency. The nominal current density, J_{nom}, is the current density necessary to excite a 1 μm-thick active layer uniformly, given unity quantum efficiency [30]. J_{th} is, then, given by the expression:

$$J_{th} = \frac{J_{nom}d}{\eta_i} \tag{2.1}$$

where:
$\quad J_{th}$: threshold current density (per unit area)
$\quad J_{nom}$: nominal current density (per unit volume)
$\quad d$: total active region thickness
$\quad \eta_i$: internal quantum efficiency

Applying this equation to the VCSEL geometry will optimize threshold current density, and provide the means to choose the correct design parameters for the VCSEL.

The threshold for lasing in the cavity is reached when the light traversing the cavity makes a round trip without attenuation. The expression for this condition can be found in most introductory semiconductor laser texts [30:Chapter 7]:

$$R_b R_f e^{2(\Gamma g_{th} - \alpha)l} = 1 \tag{2.2}$$

or, taking the natural logarithm and rearranging:

$$\Gamma g_{th} = \alpha + \frac{1}{2l} \ln\left[\frac{1}{R_b R_f}\right] \tag{2.3}$$

where:
  R_b: reflectivity of the back mirror
  R_f: reflectivity of the front mirror
  Γ: confinement factor
  g_{th}:   threshold gain of the region
  α: loss per unit length of the region
  l: length of the cavity

Equation 2.3 is the focus of this chapter. Dramatic improvements in VCSEL threshold current density stem from relatively straightforward improvements in cavity design, active region design, and mirror selection. All of these improvements reduce to an action on one of the parameters in equation 2.3. The following sections discuss the underlying theory behind these improvements and how the designs for the structures grown for this thesis effort benefit from them. Recent improvements in cavity design include the Periodic Gain Structure (PGS), discussed briefly in chapter 1. Active region improvements include Quantum Well (QW) active regions, and strained-layer effects. In mirror design, the use of distributed Bragg reflector mirrors was an early improvement to the first [29] VCSEL designs, but a description of the theory is included here to complete the treatment of the entire VCSEL structure.

2.2 Cavity Design

Ornate cavity designs for VCSELs are not essential to lasing. A simple block of bulk active material (e.g. GaAs) has been successfully used in VCSEL design from the VCSEL's inception. This type of cavity design is now referred to as the Uniform Gain Structure (UGS) [11]. Periodic Gain Structures (PGS) have become more popular recently, as they can theoretically provide up to a factor of two improvement in the threshold current density without changing the component materials of the VCSEL. The PGS takes advantage of the physical dimensions of the cavity to concentrate the active region at the peaks of the cavity electromagnetic mode (see Figure 1.2). To see how, we need to look more closely at the factors involved in equation 2.3.

2.2.1 Γ: Confinement Factor

The confinement factor, Γ, determines how much of the electromagnetic field in the cavity will coincide with the active region. The confinement factor may be defined in three dimensions for the vertical cavity structure; we are interested in the Γ for the longitudinal direction of the cavity. The longitudinal confinement factor, Γ_p, is the ratio of the magnitude of the electric field in the active region to that in the overall cavity:

$$\Gamma_p = \frac{\int_{active} E^2(z)dz}{\int_L E^2(z)dz} \tag{2.4}$$

To determine Γ_p, we use an approximation of the standing wave pattern of the electric field in the cavity [11]. For high reflectance mirrors (which is usually the case in VCSELs):

$$E(z) = E_0 \cos(kz) \tag{2.5}$$

For the PGS, assuming the active regions are placed at each of the peaks of the electromagnetic mode in the cavity, the spacing of the active regions is $\lambda/2$ (see Figure 2.1). Defining the thickness of each active region in the PGS as t, and the total active region thickness as d (which is the sum of the active regions t in the cavity), the ratio of d/t is the number of periods in the standing wave pattern. This ratio is the same as the

ratio of the cavity length to one-half the lasing wavelength ($\frac{l}{\lambda/2}$). Inserting equation 2.5 into equation 2.4 and integrating over the thickness for one period [11]:

$$\Gamma_p = \frac{\frac{d}{t} \int_t E_0^2 \cos^2(kz)dz}{\frac{l}{\lambda/2} \int_{\lambda/2} E_0^2 \cos^2(kz)dz}$$

$$\Gamma_p = \frac{d}{l}\left\{1 + \frac{\sin[\pi\frac{t}{\lambda/2}]}{[\pi\frac{t}{\lambda/2}]}\right\} \equiv \frac{d}{l}\Gamma_r \qquad (2.6)$$
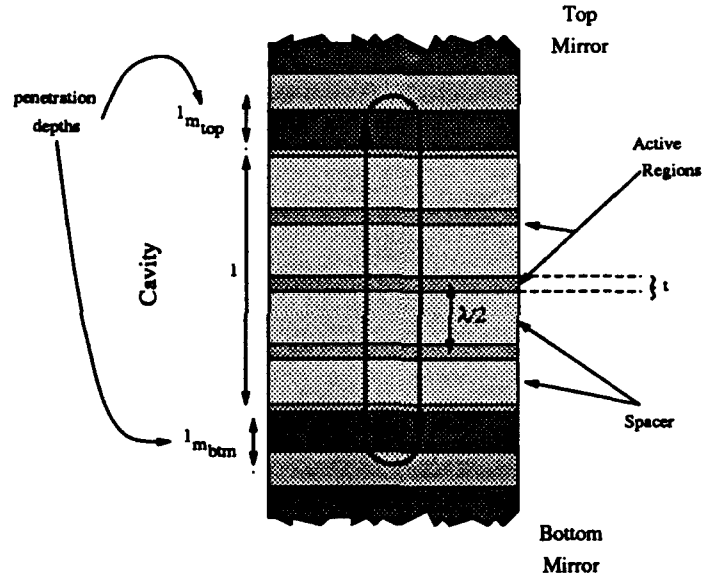
Figure 2.1. Periodic Gain Structure (PGS) VCSEL Cavity Geometry

Corzine defines Γ_r in equation 2.6 as the relative confinement factor [11]. For the situation described above, where the active regions lie at every peak of the standing wave E-field, we can equate the ratios d/t and $\frac{l}{\lambda/2}$.

$$\frac{d}{t} = \frac{l}{\lambda/2} \Rightarrow \frac{d}{l} = \frac{t}{\lambda/2} \qquad \text{active region at every peak}$$

This provides a simple equation for the relative confinement factor by substituting into equation 2.6.

$$\Gamma_r = 1 + \frac{\sin(\pi\frac{d}{l})}{(\pi\frac{d}{l})} \qquad (2.7)$$

with:
   Γ_r :   relative confinement factor
    d: total active region thickness
    l: cavity length

The factor d/l is very useful in the design of the cavity. d/l is called the *fill factor* for the cavity and represents the ratio of the active region thickness to total cavity thickness. Note that from equation 2.7 the relative confinement factor is maximized for small values of d/l. For small argument form, the term $\sin x/x \sim 1$, and the maximum value for Γ_r then, is 2 (we'll recall this later). Now, substituting $\Gamma_r d/l$ from equation 2.6 for the longitudinal confinement factor ($\Gamma = \Gamma_p$) in equation 2.3:

$$\Gamma_r g_{th} \frac{d}{l} = \alpha + \frac{1}{l}\ln[\frac{1}{R}]$$
$$\Rightarrow \Gamma_r g_{th} d = \alpha l + \ln[\frac{1}{R}] \qquad (2.8)$$

Where R is the geometric mean reflectivity of the front and back mirrors ($\sqrt{R_b R_f}$). This equation provides the relationship between the gain of the PGS active medium and the losses in the cavity and mirrors for threshold gain.

2.2.2 **Cavity losses** The losses can be further subdivided into the specific loss factors for each region of the cavity the light passes through as it makes the round trip between reflections. We can subdivide the loss term, αl into the loss in the cavity itself and the loss for the light penetrating the mirror layers adjacent to the cavity (see Figure 2.1) [9].

$$\Gamma_r g_{th} d = \alpha_i l + \alpha_m l_m + \ln[\frac{1}{R}] \qquad (2.9)$$

where:

d: total active region thickness

l_m: penetration depth of mirrors

$\Gamma_r g_{th} d$:   active region gain

$\alpha_i l$:   loss in the cavity

$\alpha_m l_m$:   mirror penetration loss

The break-out of the $\alpha_i l$ loss term in equation 2.9 includes the loss in the active and passive regions of the cavity, and loss from scattering at the sidewalls of the VCSEL [9]:

$$\alpha_i = \Gamma_p \alpha_{ia} + (1 - \Gamma_p)\alpha_{ip} + \alpha_{sc} \qquad (2.10)$$

with:

α_{ia}:   the loss per unit length in the active region

α_{ip}:   the loss per unit length in the passive region

α_{sc}:   scattering loss for the cavity

The free carrier loss for GaAs in the active elements of the structure, is given by Casey [7:p175] as:

$$\alpha_{ia} \approx 3 \times 10^{-18} n + 7 \times 10^{-18} p \qquad (2.11)$$

For $n \approx p$, as in un-doped GaAs this reduces to $\alpha_{ia}/n = 10^{-17}$.

Loss mechanisms are less well-documented for InGaAs. Coldren suggests loss factors can be as high as 100 cm^{-1} for large carrier densities. However, he later cites a typical active region loss for InGaAs as 30 cm^{-1} [9:S112].

Passive region loss and scattering loss are device dependent, for $Al_x Ga_{1-x} As$ passive regions, various authors have used from 1 to 10 cm^{-1} [28] [9]. We will use 10 cm^{-1} when we require a loss mechanism for later calculations. Scattering losses are also sparsely documented. Corzine uses an $\alpha_{sc} = 20 cm^{-1}$ as typical [11].

2.2.3 J_{th} **Design Equations** From equation 2.1 and equation 2.9 Corzine develops a useful design expression for the threshold current density. To do so we solve equation 2.9 for *d* and substitute this expression into equation 2.1.

$$
\begin{aligned}
J_{th} &= \frac{J_{nom}\,d}{\eta_i} = \frac{J_{nom}}{\eta_i}\left[\frac{\alpha_i l + \alpha_m l_m + \ln[\frac{1}{R}]}{\Gamma_r g_{th}}\right] \\
&= \frac{J_{nom}}{\eta_i}\frac{(\alpha_m l_m + \ln[\frac{1}{R}])}{\Gamma_r g_{th}}\frac{(\alpha_i l + \alpha_m l_m + \ln[\frac{1}{R}])}{(\alpha_m l_m + \ln[\frac{1}{R}])}
\end{aligned}
\tag{2.12}
$$

By rearranging and using the expression for Γ_p (equation 2.3) the resultant threshold current design equation falls out. From equations 2.3 and 2.9:

$$
\Gamma_p g_{th} l = \alpha_i l + \alpha_m l_m + \ln[\frac{1}{R}]
$$

Thus:

$$
\frac{(\alpha_i l + \alpha_m l_m + \ln[\frac{1}{R}])}{(\alpha_m l_m + \ln[\frac{1}{R}])} = \frac{\Gamma_p g_{th} l}{\Gamma_p g_{th} l - \alpha_i l} = \frac{\Gamma_p g_{th}}{\Gamma_p g_{th} - \alpha_i}
$$

Substituting this into equation 2.12:

$$
\begin{aligned}
J_{th} &= \frac{J_{nom}}{g_{th}}\frac{1}{\eta_i \Gamma_r}\frac{\ln(1/\ )}{\frac{\ln(1/R)}{\alpha_m l_m + \ln(1/R)}}\frac{\Gamma_p g_{th}}{\Gamma_p g_{th} - \alpha_i} \\
&= \frac{J_{nom}}{g_{th}}\frac{\ln(1/R)}{\eta_m \eta_i}\frac{1}{\Gamma_r}\left[1 - \frac{\alpha_i}{\Gamma_p g_{th}}\right]^{-1} \\
&= J_0(R)\frac{1}{\Gamma_r}\left[1 - \frac{\alpha_i}{\Gamma_p g_{th}}\right]^{-1}
\end{aligned}
\tag{2.13}
$$

Equation 2.13 separates the components of the threshold current density. It is useful to examine the components of equation 2.13 in more detail.

$\frac{J_{nom}}{g_{th}} \frac{\ln(1/R)}{\eta_m \eta_i}$ This is the normalization constant $J_0(R)$ and represents the current density which will normalize the threshold current density J_{th} for no internal losses ($\alpha_i = 0$) and for a relative confinement factor $\Gamma_r = 1$ (Note: this infers the fill factor $d/l = 1$, corresponding to Uniform Gain Structure (UGS) active medium)

Γ_r The relative confinement factor, as noted before, has a maximum value of 2, indicating a potential for Γ_r to halve the threshold current density.

$\frac{J_{nom}}{g_{th}}$ ratio of the nominal current density to the threshold gain. By minimizing this factor, we may minimize J_{th}

Efficiencies: Although it is unnecessary to separate the efficiencies of the cavity, mirror, and active regions, it can be helpful in relating design efforts, to compare mirror efficiencies for a design using varying concentrations of Aluminum, for example. The various efficiencies for the structure are explained below

η_m: the conversion efficiency of the mirrors is given by the equation:

$$\eta_m = \frac{\ln(1/R)}{\alpha_m l_m + \ln(1/R)}$$

and is 1 for no mirror penetration loss ($\alpha_m l_m = 0$).

η_i: internal quantum efficiency (for the active region only)

η_c: the cavity efficiency, together with the mirror efficiency η_m provide the external efficiency η_{ex} of the structure (ratio of output loss though mirrors to total loss (cavity and mirrors)):

$$
\begin{aligned}
\eta_{ex} &= \frac{\ln[\frac{1}{R}]}{\alpha_i l + \alpha_m l_m + \ln[\frac{1}{R}]} &= \eta_m \frac{\alpha_m l_m + \ln[\frac{1}{R}]}{\Gamma_p g_{th}} \\
&&= \eta_m \left[1 - \frac{\alpha_i}{\Gamma_p g_{th}}\right] \\
&&= \eta_m \eta_c \\
\Rightarrow \eta_c &= 1 - \frac{\alpha_i}{\Gamma_p g_{th}} && (2.14)
\end{aligned}
$$

2.3 Active Region Design

VCSEL active region design improvements have fed off improvements in active regions for in-plane semiconductor lasers. The addition of multiple quantum wells and strained layers led to improved threshold current densities in addition to those attainable by the PGS structure presented in the previous section. It is instructive to first examine the contribution of plain bulk active regions to the PGS structure, then note how QWs can improve performance:

2.3.1 Bulk Active Regions

For bulk active regions, to obtain the minimum J_{th} we need to determine the minimum normalization constant $J_0(R)$. To this end, we need to maximize η_m, η_i, and R, and minimize J_{nom}/g_{th} in equation 2.13. Of these parameters, active region design influences J_{nom}/g_{th} most.

To illustrate, the process for a GaAs active region follows. A derivation for the linear relationship between gain and carrier density for GaAs can be found in Yariv [33:p564].

$$g = a(n - n_{tr}) \tag{2.15}$$

with:
- n carrier density in the material
- n_{tr} carrier density necessary for transparency
- a curve fitting constant

From McIlroy [27] for small dopant levels ($n \approx p$) the nominal current density can be given by the equation:

$$J_{nom} = eB_{eff}n^2 \tag{2.16}$$

with:
- e electron charge
- B_{eff} recombination rate

By solving equations 2.16 and 2.15 for n, and equating the resultant expressions, we can obtain an expression for g in terms of J_{nom}:

$$J_{nom} = eB_{eff}n^2 \Rightarrow n = \sqrt{\frac{J_{nom}}{eB_{eff}}}$$

$$g = a(n - n_{tr}) \Rightarrow n = \frac{g}{a} + n_{tr}$$

$$\Rightarrow g = a[\sqrt{\frac{J_{nom}}{eB_{eff}}} - n_{tr}] \qquad (2.17)$$

Corzine assigns the following values to the constants in this equation [11]:

a: $2.5 \times 10^{-16} cm^2$
B_{eff}: $10^{-10} cm^3/s$
n_{tr}: $1.5 \times 10^{18} cm^{-3}$

With these assignments, a graph of the gain vs values of J_{nom} illustrates their interdependence (see Figure 2.2)
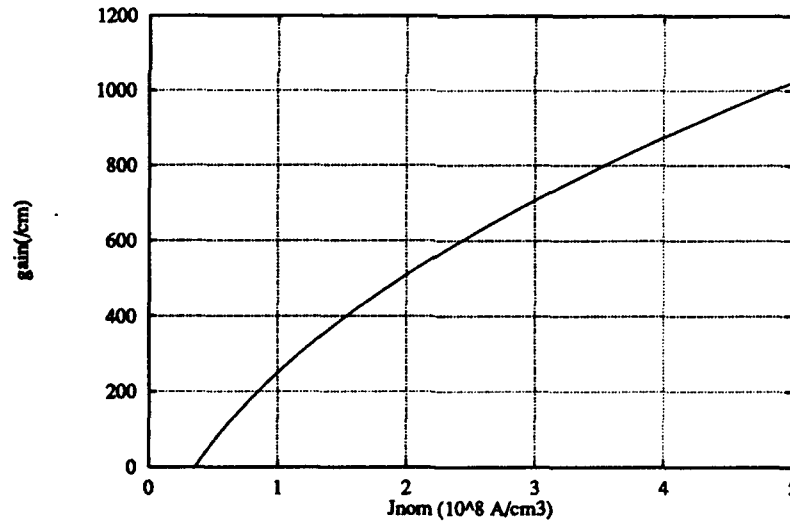
Figure 2.2. Gain vs Nominal Current Density Curve for GaAs

By dividing both sides of equation 2.17 by J_{nom} we can also plot g/J_{nom} vs J_{nom} (see Figure 2.3)

If we maximize g/J_{nom} from figure 2.3, this fixes J_{nom}; we can then extract the corresponding gain from figure 2.2. As a first estimate, Corzine suggests the value for the
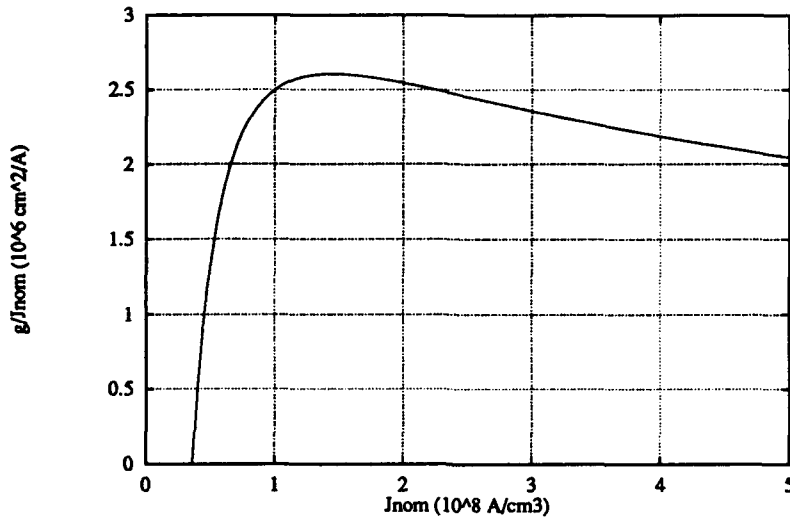
Figure 2.3. g/J_{nom} vs J_{nom} Curve for GaAs

gain should be chosen on the high side of the peak in figure 2.3 [11]. By doing so the gain will help to minimize the effects of internal loss in the cavity efficiency (see equation 2.14).

d/l: *Fill Factor Choice* The fill factor choice is the first point in the analysis where the improvement in efficiency is dramatically evident. Using equation 2.13, we can write the ratio of the threshold current density to the normalization constant as:

$$\frac{J_{th}}{J_0(R)} = \frac{1}{\Gamma_r}\left[1 - \frac{\alpha_i}{\Gamma_p g_{th}}\right]^{-1} \tag{2.18}$$

For example, in GaAs, we can determine an optimal fill factor. Assume reasonable internal losses ($\alpha_{ip} = 10cm^{-1}$, $\alpha_{sc} = 20cm^{-1}$: see *Cavity Losses* above). Determine the optimal gain by choosing a J_{nom} in figure 2.3 which produces a maximum in g/J_{nom}. Now use this J_{nom} to determine the gain from figure 2.2. The result is a J_{nom} between $1.2 \times 10^8 A/cm^3$ and $1.8 \times 10^8 A/cm^3$, and corresponds to a threshold gain in the vicinity of 350 to 500 cm^{-1}. As noted before, Corzine [11] advises the gain should be chosen near the high end of this range, to minimize losses. Assigning a gain of 500 cm^{-1}, we can determine the carrier density n from equation 2.15. With the constants a and n_{tr} as defined before,

the gain of 500 cm^{-1} implies $n = 3.5 \times 10^{18}$. Now insert this value (assume $n \approx p$ true for un-doped material) into the expression for the free carrier absorption in equation 2.11:

$$
\begin{aligned}
\alpha_{ia} &= n \times 10^{-17} \\
&= 35 cm^{-1}
\end{aligned}
$$

Returning to equation 2.18, if we plug in the expressions for α_i from equation 2.10, and Γ_p from equation 2.6:

$$
\begin{aligned}
\frac{J_{th}}{J_0(R)} &= \frac{1}{\Gamma_r}\left[1 - \frac{\Gamma_p\alpha_{ia} + (1 - \Gamma_p)\alpha_{ip} + \alpha_{sc}}{\Gamma_p g_{th}}\right]^{-1} \\
&= \frac{1}{\Gamma_r}\left[1 - \frac{\Gamma_r(d/l)\alpha_{ia} + (1 - \Gamma_r(d/l))\alpha_{ip} + \alpha_{sc}}{\Gamma_r(d/l)g_{th}}\right]^{-1}
\end{aligned}
\tag{2.19}
$$

Finally, using Γ_r from equation 2.7:

$$
\Gamma_r = 1 + \frac{\sin(\pi\frac{d}{l})}{(\pi\frac{d}{l})}
$$

We can plot equation 2.19 vs fill factor d/l.

The plot (see figure 2.4) illustrates how the correct choice of the fill factor can improve the threshold current density. *Unit gain* in the graph represents the gain for a UGS GaAs active region with no loss. The dip in the curve represents a 40 % reduction in the threshold current density for a periodic Gain Structure (PGS) *including loss* over a Uniform Gain Structure (UGS) with no loss.

2.3.2 **Quantum Well Active Regions** Quantum well active regions can provide additional reductions in threshold current density. For both In$_x$Ga$_{1-x}$As and GaAs, the optimal gain of the QW is dependent on the well width. A brief background in quantum well theory is in order to determine how to make informed choices concerning quantum well parameters.
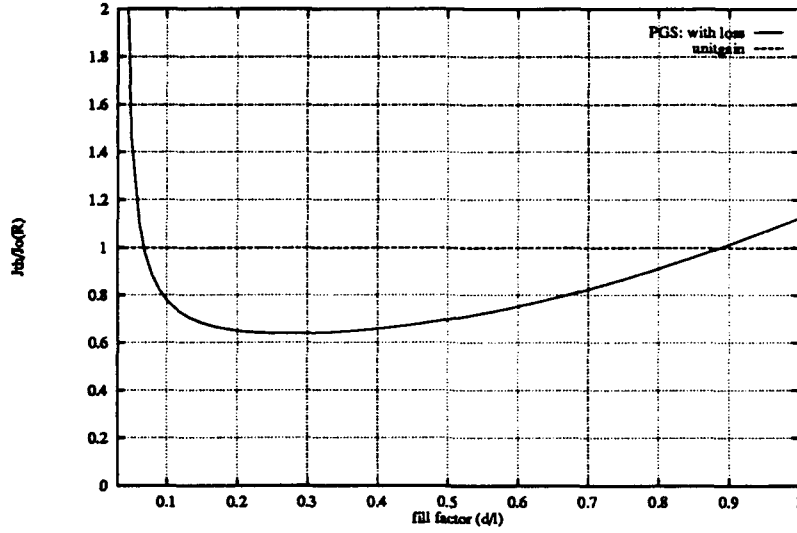
Figure 2.4. $J_{th}/J_0(R)$ vs Fill Factor(d/l) Curve for GaAs

Transition Energy   The transition energy in quantum wells is comprised of four primary contributors [32] (see figure 2.5).

$$E = h\nu = E_G + E_{conf}^c + E_{conf}^v - E_{exc} \tag{2.20}$$

where:
  - h: Boltzman's constant
  - ν: frequency of the transition
  - E_G: energy gap of the bulk semiconductor
  - E_{conf}^c: confinement energy of the conduction band
  - E_{conf}^v: confinement energy of the valence band
  - E_{exc}: exciton absorption energy

Gap Energy   The energy gap for $In_x Ga_{1-x}As$ and $Al_x Ga_{1-x}As$ bulk active regions depend on the concentrations of the Indium (or Aluminum) in the ternaries. The $In_x Ga_{1-x}As$ parameters for this effort were obtained from Kolbas [22], while the $Al_x Ga_{1-x}As$ parameters were gotten from Adachi [2]
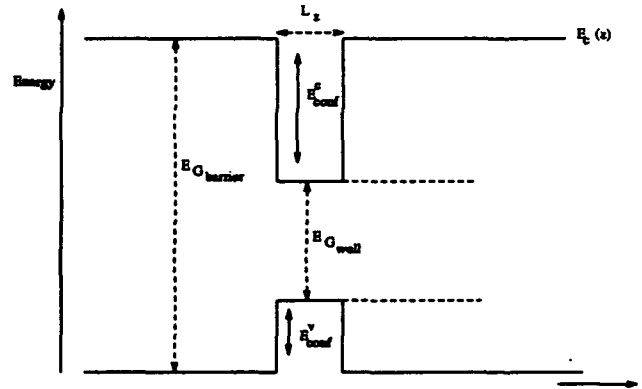
Figure 2.5. Quantum Well Energy Diagram

Electron Confinement Energy The electron confinement energy can be calculated using the infinite well approximation. For initial calculations we take the energy difference ΔE_c between the conduction bands of the well and the barriers to be infinite. Modelling the energy in the system with the Schrödinger equation; we have, for the conduction band:

$$V(z)u(\mathbf{r}) - \frac{\hbar}{2m_c^*}\nabla^2 u(\mathbf{r}) = Eu(\mathbf{r}) \tag{2.21}$$

where:
  $V(z)$: potential energy function confining the electrons in the z direction
  $u(\mathbf{r})$: wavefunction for the electrons in the well
  E: energy of the electron
  m_c^*: effective mass of the electron

Applying separation of variables to solve the equation, the eigenfunction $u(\mathbf{r})$ can be written as the product:

$$u(\mathbf{r}) = \psi_k(\mathbf{r}_\perp)u(z) \tag{2.22}$$

...with $\mathbf{r}_\perp$ the component of $\mathbf{r}$ perpendicular to the $\hat{z}$ direction (in the plane of the well). By inserting this relation into equation 2.21 and extracting the z-dependent portion we obtain a 1-D wave equation:

$$V(z)\psi_k(\mathbf{r}_\perp)u(z) - \frac{\hbar}{2m_c^*}\nabla^2\psi_k(\mathbf{r}_\perp)u(z) = E\psi_k(\mathbf{r}_\perp)u(z)$$

$$\Rightarrow \left[V(z) - \frac{\hbar}{2m_c^*}\nabla^2\right]\psi_k(\mathbf{r}_\perp)u(z) = E\psi_k(\mathbf{r}_\perp)u(z)$$

$$\Rightarrow V(z) - \frac{\hbar}{2m_c^*}\left[\frac{1}{u(z)}\frac{\delta^2(u(z))}{\delta z^2} + \frac{1}{\psi_k(\mathbf{r}_\perp)}\frac{\delta^2(\psi_k(\mathbf{r}_\perp))}{\delta x^2} + \right.$$
$$\left. \frac{1}{\psi_k(\mathbf{r}_\perp)}\frac{\delta^2(\psi_k(\mathbf{r}_\perp))}{\delta y^2}\right] = E$$

Now, extracting the z-dependent component:

$$\left[V(z) - \frac{\hbar}{2m_c^*}\frac{\delta^2}{\delta z^2}\right]u(z) = E_z u(z) \tag{2.23}$$

For well width L_z, $u(z)$ must vanish at the walls ($z = \pm L_z/2$) for the equation to remain bounded, since

$$\lim_{z \to \pm\frac{L_z}{2}} V(z) \to \infty$$

with this boundary condition:

$$u_l(z) = \begin{cases} \cos l\frac{\pi}{L_z}z & l = 1,3,5,\ldots \\ \sin l\frac{\pi}{L_z}z & l = 2,4,6,\ldots \end{cases} \tag{2.24}$$

Solving for the constant E_z when $V(z) = 0$ (in the well)

$$E_z = l^2\frac{\hbar^2\pi^2}{2m_c^*L_z^2} \qquad l = 1,2,3\ldots \tag{2.25}$$

The energy for the x and y components in equation 2.21 are determined by solving for $\psi(\mathbf{r}_\perp)$ as a two dimensional Bloch wavefunction [33:Chapter 15]. The wavefunction of the electron in the conduction band is characterized by the wave vector $\mathbf{k}_\perp$ and a Bloch wavefunction:

$$\psi(\mathbf{r}_\perp) = u_{\mathbf{k}_\perp}(\mathbf{r}_\perp)e^{(i\mathbf{k}_\perp \cdot \mathbf{r}_\perp)} \tag{2.26}$$

The expression of the overall energy of the electron characterized by the vector $\mathbf{k}_\perp$ as measured from the bottom of the band is [33]:

$$E(\mathbf{k}_\perp) = \frac{\hbar^2 k_\perp^2}{2m_c^*} \tag{2.27}$$

By adding the energies in equation 2.25 and equation 2.27, the overall energy above the conduction band becomes:

$$E_{conf}^c(\mathbf{k}_\perp, l) = E_z + E(\mathbf{k}_\perp) = \frac{\hbar^2 k_\perp^2}{2m_c^*} + l^2 \frac{\hbar^2 \pi^2}{2m_c^* L_z^2} \tag{2.28}$$

Hole Confinement Energy The hole quantization problem is more difficult, a result of the degeneracy of the valence subbands. The more rigorous methods used to characterize the energies in the valence band for light and heavy hole masses use the Kane model [32]. This model describes the valence bands using basis functions with angular momentum symmetry ($J = \pm\frac{3}{2}, \pm\frac{1}{2}$). This equates to 4-fold degeneracy at $k = 0$. The basis functions are described by the *Luttinger-Hamiltonian*, and an explicit development is contained in Weisbuch. The resultant energies for the light and heavy hole confinement energies are [32]:

$$E_{conf}^{vl}(\mathbf{k}_\perp, l) = \frac{\hbar^2 k_\perp^2}{2m_0}(\gamma_1 - \gamma_2) + l^2 \frac{\hbar^2 \pi^2}{2m_0 L_z^2}(\gamma_1 - \gamma_2) \tag{2.29}$$

$$E_{conf}^{vh}(\mathbf{k}_\perp, l) = \frac{\hbar^2 k_\perp^2}{2m_0}(\gamma_1 + \gamma_2) + l^2 \frac{\hbar^2 \pi^2}{2m_0 L_z^2}(\gamma_1 + \gamma_2) \tag{2.30}$$

where:
E_{conf}^{vl}: light hole confinement energy
E_{conf}^{vh}: heavy hole confinement energy
$\gamma_{1,2}$: Luttinger parameters
m_0: electron rest mass

The Luttinger parameters can be used to obtain the effective mass for the valence band light (m_{lh}) and heavy (m_{hh}) holes in the strained quantum well [12]:

$$m_{hh} = m_0 \frac{1}{\gamma_1 - \gamma_2}$$

$$m_{lh} = m_0 \frac{1}{\gamma_1 + \gamma_2}$$

These forms are convenient if the Luttinger parameters can be obtained for the active region materials involved, one source for Luttinger parameters in III-V compounds is Landolt-Bornstein [24].

Exciton Energy   The electron and hole pairs in the conduction and valence bands are correlated in their motion [32]. This correlation can be modeled as a simple Coulomb attraction of the electron-hole pair (also referred to as an exciton). The effect of this interaction produces the exciton binding energy E_{exc} in equation 2.20. The exciton effect is not significant in lasers, where high injection of charged carriers screens the Coulomb interaction [5]. For this reason we will assume $E_{exc} \sim 0$.

The total transition energy is the sum of the energies in equation 2.20. With $E_{exc} \sim 0$:

$$
\begin{aligned}
h\nu &= E_G + E_{conf}^c(\mathbf{k}, l) + E_{conf}^v(\mathbf{k}, l) \\
&= E_G + \left(\frac{1}{m_c^*} + \frac{1}{m_0}(\gamma_1 \pm \gamma_2) \right) \frac{\hbar^2}{2} \left(k^2 + l^2 \frac{\pi^2}{L_z^2} \right) \\
&= E_G + \frac{\hbar^2}{2m_r} \left(k^2 + l^2 \frac{\pi^2}{L_z^2} \right)
\end{aligned}
\tag{2.31}
$$

where:
  E_G: energy gap of the bulk well material
  L_z: well width
  m_r: reduced mass of the electron - hole pair
  l: 1,2,...
  k: 0,1,2,...

Quantum Well Barriers The barriers must have a sufficiently large energy gap above that of the wells to contain the carriers. In addition the barriers must separate the wells to prevent inter-well coupling, which can negate quantum effects [32]. Jewell [19] suggests barrier widths of 100 Å, and Corzine [10] recommends the conduction band barrier height be kept 100 meV above the well.

Strain Effects Lattice strain in the active layers can alter the dispersion of the valence band energies. For GaAs and $In_x Ga_{1-x}As$ active regions on GaAs substrates, compressive strain (see figure 2.6 [10]) tends to elevate the heavy-hole valence band above the light-hole valence band. The result is less band mixing in the valence band. This makes the bands more parabolic and decreases the density of states in the upper valence bands. The lightened upper valence band density of states reduces the current density for transparency (J_{tr}), lowering the threshold current density.
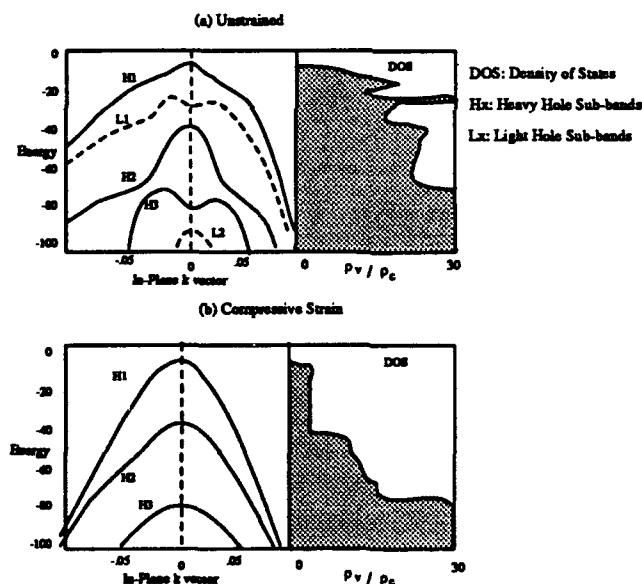
Figure 2.6. Compressive Strain Effects on Valence Sub-Bands (GaAs) [After Corzine[10]]

Strain for InGaAs wells on GaAs substrate is compressive for any Indium x concentration. $In_x Ga_{1-x}As$ wells on InP substrate produce either tensile (for $x < .532$) or compressive $(x > .5321)$ strain.

Critical Thickness It is important in strained layer design to be certain the layer thickness does not exceed the critical layer thickness. The critical layer thickness for the lattice is a function of the strain and the layer thickness. Exceeding this thickness forms dislocations in the growth surface which propagate to the interface, forming uneven layer growth [22]. If using $In_xGa_{1-x}As$, to achieve the desired transition energy, the designer must pick a well width L_z and an Indium concentration x. The x concentration affects E_G, m_v and m_c^* in equation 2.31. It also affects the strain between layers, so given a well width, there will be a limit on x concentrations which will produce layers below the critical layer thickness. Fritz characterizes $In_xGa_{1-x}As$ for critical thickness vs strain for strain values of 0.5 % to 3 % and for layer thicknesses from 50 to 500 Å[15].

Polarization Polarization of the output beam is usually attributed to strain in the active regions [14]. The strain in InGaAs/GaAs and InGaAs/InGaAsP quantum wells has been shown to produce significant polarization effects. Transverse electric (TE) peak gain is usually defined as corresponding to the gain seen by an optical field with its electric field polarized in the plane of the well. Transverse magnetic (TM) peak gain corresponds to the electric field perpendicular to the plane of the well. Ahn and Chuang [3] link TM gain to the relative dominance of light hole sub-bands in the quantum well; while they attribute TE gain to heavy hole sub-band dominance. For this reason, compressive strain as shown in figure 2.6 tends to favor TE gain. Tensile strain has been shown to raise the light hole sub-bands in InGaAs, and produced predominantly TM polarized light [10].

2.4 Mirror Design

The distributed Bragg reflector mirror design has been prevalent in VCSEL structures since the late 70's. This section describes the transmission matrix approach to calculating mirror reflectivities, and discusses the effects of the penetration depth of the electromagnetic mode into the cavity.

2.4.1 Transmission Matrix The transmission matrix approach to reflectivity calculations models the multiple reflections in the multilayer medium as two lumped optical

fields: one traveling in the positive direction, and one in the negative, or reflected, direction. The positive going electric and magnetic field vectors in the mth layer are denoted by E_m^+ and H_m^+. The reflected fields are denoted by E_m^- and H_m^-. The total field in the mth layer can then be written [25]:

$$
\begin{aligned}
E_m &= E_m^+ + E_m^- \\
H_m &= \mu_m(E_m^+ - E_m^-)
\end{aligned}
\tag{2.32}
$$

Where the final equality uses the (possibly complex) effective refractive index (μ_m) of the mth layer to relate the E and H fields. The effective indices in the mirror layers is derived from the complex refractive index (n_m) and the angle of incidence (θ_m):

$$
\begin{aligned}
\mu_m &= n_m / \cos\theta_m, \quad \text{for the } p\text{-component of polarization} \\
\mu_m &= n_m \cos\theta_m, \quad \text{for the } s\text{-component of polarization}
\end{aligned}
\tag{2.33}
$$

θ_m can of course be related to the external angle of incidence (θ_0) (see figure 2.7) and the angle of the beam in the substrate (θ_{sub}) by Snell's law. The phase of the light as it traverses the mth layer is determined by the equation:

$$
\delta_m = \frac{2\pi n_m d_m \cos\theta_m}{\lambda}
\tag{2.34}
$$

where:
  δ_m: phase of the field
  d_m: physical thickness of the layer
  λ: free space wavelength of the light

Following the matrix method developed by Heavens, [18], we apply boundary conditions to the E and H fields incident at the interfaces. Namely, these fields must be continuous across the boundaries. The matrix solution to this boundary value problem is of the form:
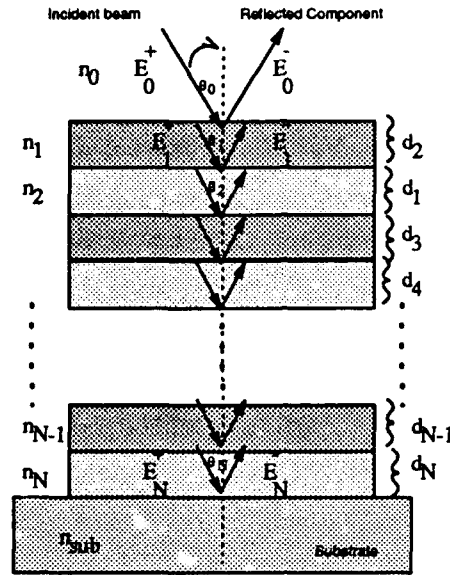
Figure 2.7. Geometry for Reflected Fields in Multilayer Stack

$$\begin{pmatrix} E_{m-1}^{+} \\ E_{m-1}^{-} \end{pmatrix} = \begin{bmatrix} \cos \delta_m & \frac{i}{\mu_m} \sin \delta_m \\ i\mu_m \sin \delta_m & \cos \delta_m \end{bmatrix} \begin{pmatrix} E_m^{+} \\ E_m^{-} \end{pmatrix} \tag{2.35}$$

In this form, we can easily extend the application to an N layer stack:

$$\begin{pmatrix} E_0 \\ H_0 \end{pmatrix} = \prod_{m=1}^{N} \mathbf{M_m} \begin{pmatrix} E_N \\ H_N \end{pmatrix} \tag{2.36}$$

with $\mathbf{E_0}$ and $\mathbf{H_0}$ the incident electric and magnetic fields and the characteristic matrix:

$$\mathbf{M_m} = \begin{bmatrix} \cos \delta_m & \frac{i}{\mu_m} \sin \delta_m \\ i\mu_m \sin \delta_m & \cos \delta_m \end{bmatrix}$$

We are interested, for the VCSEL mirrors, in the reflectivity in a stack composed of quarter-wave thicknesses (each layer has $d_m = \lambda/4$). For this thickness the phase δ_m

becomes:

$$\delta_m = \frac{2\pi n_m d_m \cos\theta_m}{\lambda} = \frac{\pi \cos\theta_m}{2} \qquad (2.37)$$

For normal incidence, $(\theta_m = 0)$, this results in a value of $\delta_m = \frac{\pi}{2}$. So the characteristic matrix $\mathbf{M}_m$ reduces to:

$$\mathbf{M_m} = \begin{bmatrix} 0 & \frac{i}{\mu_m} \\ i\mu_m & 0 \end{bmatrix} \qquad \text{normal incidence, } d_m = \lambda/4$$

From this matrix expression, we can determine the exiting fields from the quarter-wave stack; for N layers and the substrate:

$$\begin{pmatrix} E_0 \\ H_0 \end{pmatrix} = \prod_{m=1}^{N+sub} \mathbf{M_m} \begin{pmatrix} E_{sub} \\ H_{sub} \end{pmatrix} = \prod_{m=1}^{N+sub} \begin{bmatrix} 0 & \frac{i}{\mu_m} \\ i\mu_m & 0 \end{bmatrix} \begin{pmatrix} 1 \\ \mu_{sub} \end{pmatrix} E_{sub} \qquad (2.38)$$

The reflectivity is then given by [25]:

$$\Re = \left| \frac{\mu_0 E_0 - H_0}{\mu_0 E_0 + H_0} \right|^2 = \left| \frac{\mu_0 - H_0/E_0}{\mu_0 + H_0/E_0} \right|^2 \qquad (2.39)$$

Once the product of the matrices in equation 2.38 is determined, the ratio $H_0/E_0 = Y$, where Y is the optical admittance follows. This results in two cases (for N odd or even):

$$Y = \begin{cases} \dfrac{\mu_1^2 \mu_3^2 \cdots \mu_N^2}{\mu_2^2 \mu_4^2 \cdots \mu_{sub}} & N \text{ odd} \\[2em] \dfrac{\mu_1^2 \mu_3^2 \cdots \mu_{N-1}^2 \mu_{sub}}{\mu_2^2 \mu_4^2 \cdots \mu_N^2} & N \text{ even} \end{cases} \qquad (2.40)$$

And the reflectivity is a straightforward calculation [25]:

$$\Re = \left| \frac{\mu_0 - Y}{\mu_0 + Y} \right|^2 \qquad (2.41)$$

The choice of materials in the layers dictates the values of Y. The object is to have $Y >> \mu_0$ or $Y << \mu_0$ to make $\Re \approx 1$; to do so one must choose the layers adjacent to the substrate, and incident medium, so that the change in refractive index is maximized at these interfaces. This will determine whether N will be even or odd in equation 2.40. The number of even or odd layers will then determine the admittance and reflectivity to be attained.

2.4.2 **Refractive Indices** The VCSEL mirrors in this thesis effort used varying concentrations of $Al_x Ga_{1-x} As$. The material parameters based on x concentration for $Al_x Ga_{1-x} As$ were obtained from Adachi [2].

The refractive index is taken as the square root of the real part of the dielectric constant:

$$n(\omega) \simeq \sqrt{\epsilon_1(\omega)}$$

with:
  $n(\omega)$:   frequency dependent index of refraction
  $\epsilon_1(\omega)$:   frequency dependent real part of dielectric constant

And $\epsilon_1(\omega)$ for AlGaAs can be expressed as [2]

$$\epsilon_1(\omega) = A_0(x) \left\{ f(\chi) + \frac{1}{2} \left[E_0/(E_0 + \Delta_0) \right]^{3/2} f(\chi_{so}) \right\} + B_0(x) \tag{2.42}$$

In equation 2.42 the components are defined:

$$
\begin{aligned}
f(\chi) &= \chi^{-2} \left[2 - (1 + \chi)^{1/2} - (1 - \chi)^{1/2} \right] \\
\chi &= \hbar\omega/E_0 \\
\chi_{so} &= \hbar\omega/(E_0 + \Delta_0)
\end{aligned}
$$

where:
  E_0:   direct band gap energy
  Δ_0:   spin orbit split-off energy
  A_0, B_0:   x-dependent constants

These parameters may be expressed in terms of the x concentration of the material as [2]:

$$E_0 = 1.425 + 1.155x + 0.37x^2 \quad \text{eV}$$

$$E_0 + \Delta_0 = 1.765 + 1.115x + 0.37x^2 \quad \text{eV}$$

$$A_0 = 6.30 + 19.0x$$

$$B_0 = 9.4 - 10.2x$$

2.4.3 **Reflectivity Calculations** The above equations were used to calculate the reflectivity spectra for the VCSEL structures measured and designed for this thesis effort. The program used was developed initially at the University of Arizona. The algorithm is designed for $Al_x Ga_{1-x} As$ mirror layers and cavity materials, but should work reasonably well for cavities containing InGaAs, which has a refractive index reasonably close to that of GaAs. The algorithm is fairly simple and is explained by the process below:

1. Read in the number of layers in the top and bottom mirrors and the Aluminum concentrations in the high and low index layers.

2. Read in the length of the cavity, the Aluminum concentration of the cavity, and the lasing wavelength. (Note: The Periodic Gain Structure will add layers to the internal structure of the cavity. For this analysis, the relatively close index match between InGaAs and GaAs in the cavity provides a negligible effect on the spectral reflectance of the structure, and is not considered in the analysis.)

3. Using the above data calculate the refractive index (n_m) via the above equations. From n_m and the angle of incidence, the effective index (μ_m) may be determined using equation 2.33.

4. Next, calculate the phase change via equation 2.34 above for each successive layer, then determine the admittance Y (equation 2.40) from them; finally, insert Y into equation 2.41 to produce the desired reflectivity.

Programs to calculate the reflectivity of a single multi-layer stack and for a vertical cavity structure are contained in Appendix A.

2.4.4 Spectral Reflectivity Stop Band

MacLeod recounts the derivation for the calculation of the stop band for the quarter wave DBR reflector from the indices of refraction for the two layers in the stack. The relation is given by [26]:

$$\frac{\Delta\omega}{\omega_0} = \frac{4}{\pi}\sin^{-1}\left(\frac{n_H - n_L}{n_H + n_L}\right) \tag{2.43}$$

where:
- $\Delta\omega$:   stop band width (frequency)
- ω_0:   center frequency
- n_H, n_L: high and low indices for the layers

From equation 2.43, it is evident that the layer thicknesses do not affect the stop band width, and that changes in the index of refraction for one or both of the layers can affect it considerably. Variations in x concentration can result in significant changes in the indices of the layers, narrowing or broadening the stop band. As a result, the stop band width provides an effective indication of the control of x concentration in the layers, regardless of how precise the control on layer thickness.

Equation 2.43 provides a rough estimate for the expected stop band width for the structure. In practice, dispersion will limit its effectiveness. To account for dispersive effects, calculations for spectral reflectivity, and, as a result, stop band width, should be completed via the matrix method described earlier. The FORTRAN programs in Appendix A use the matrix method.

2.4.5 Penetration Depth

The penetration of the optical mode into the mirrors will affect the loss (through the $\alpha_m l_m$ term) in equation 2.9, and the effective cavity length. Both of these concerns are addressed in this section.

Reflection Delay   The reflection delay τ_r is used to express the change in phase of the optical field upon reflection from the mirror. To illustrate, figure 2.8 shows an equivalent fixed phase mirror model of the cavity/mirror interface [4].
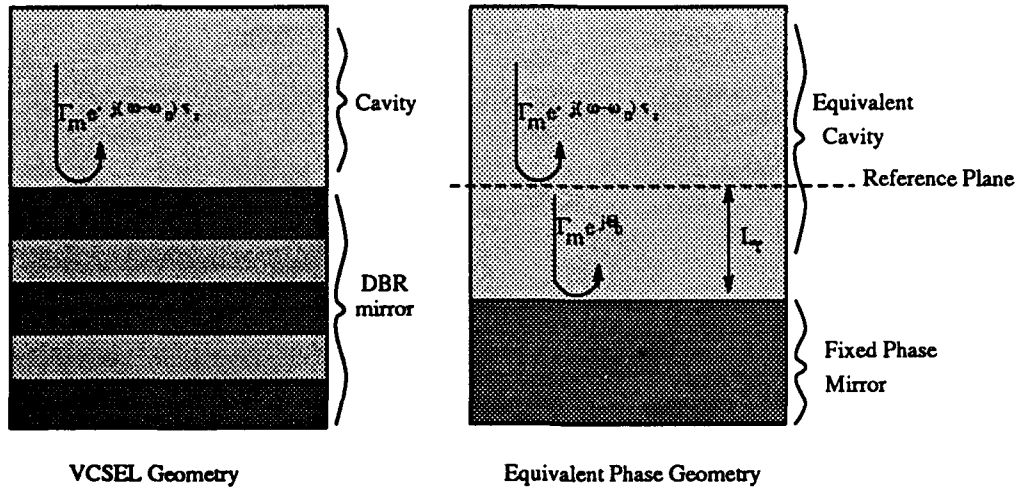
Figure 2.8. Equivalent Fixed Phase Mirror Model for Determining Reflection Delay in Multilayer Stack [After Babic [4]]

For the linear phase mirror at the top of figure 2.8, the observer above the mirror surface sees a reflected optical field which has changed in amplitude and phase. The amplitude change is modeled by the reflection coefficient (Γ_m), while the phase change is taken into account by the $(\omega - \omega_0)\tau_r$ factor in the exponential. Here, ω is the frequency of the incident light, while ω_0 is the Bragg frequency (center frequency of the reflectivity stop band). The result is no phase change for center Bragg frequency $(\omega = \omega_0)$. This is consistent with the mirror design, since the $\lambda/4$ layers are designed to have identical phase (0 or π) at each alternating layer at the Bragg frequency. Thus the light entering at the Bragg frequency should have the same phase when it exits the mirror. Wavelengths which are removed from the center frequency experience the linear phase shift described by the frequency difference and reflection delay in the exponential $((\omega - \omega_0)\tau_r)$.

The second diagram in figure 2.8 models the linear phase mirror as a fixed phase mirror set back from the observer's point of view a distance L_r. The recovered distance (L_r) is the penetration depth (sometimes called the *phase* penetration depth). The refractive index in this recovered length is the same as that in the observer's medium.

For $Al_xGa_{1-x}As$, the index differences in the high (n_N) and low (n_L) index mirror layers is small compared to the average index of the layers ($n_H - n_L \ll n_{av}$). The reflection

delay τ_r for small index differences ($n_{av} \approx n$, the index of the cavity) has been obtained via coupled wave theory [23] as:

$$\tau_r = \frac{n}{c} \frac{\tanh \kappa l}{\kappa} \tag{2.44}$$

where:
  τ_r: reflection delay
  n: index of refraction of the cavity
  c: speed of light (free space)
  κ: coupling coefficient
  l: mirror length

The coupling coefficient (κ) for square wave perturbations (as for abrupt index changes in mirror layers) is $\kappa = 2\Delta n/\lambda_0$. Here Δn is the refractive index difference ($n_H - n_L$) in the mirror layers, and λ_0 is the Bragg frequency.

Phase Penetration Depth From figure 2.8 it is a simple exercise to determine the penetration depth and fixed phase of the mirror. The phase penetration depth is just the distance the light travels in the medium:

$$L_\tau = \frac{c\tau_r}{2n}$$

... and the fixed phase of the mirror can be determined by equating the two reflected fields.

$$\Gamma_m e^{-j(\omega-\omega_0)\tau_r} = e^{j\beta 2L_r} \Gamma_m e^{j\Theta_0} \tag{2.45}$$

... with $\beta = n\omega/c$ the propagation coefficient of the mode. Now substitute for L_r and solve for Θ_0:

$$\Gamma_m e^{-j(\omega-\omega_0)\tau_r} = \Gamma_m e^{-j(\beta 2L_r - \Theta_0)}$$

$$\Rightarrow (\omega - \omega_0)\tau_r = 2\frac{n\omega}{c}\frac{c\tau_r}{2n} - \Theta_0$$

$$\Rightarrow \omega_0 \tau_r = \Theta_0 \qquad (2.46)$$

The sum of the phase terms in the equivalent fixed phase mirror cavity can be equated to an integer multiple of 2π to determine the electromagnetic modes of the cavity [4]:

$$2\beta(L_{FP} + L_{\tau_{back}} + L_{\tau_{frnt}}) - \omega_0 \tau_{r(back)} - \omega_0 \tau_{r(frnt)} = 2\pi k \qquad (2.47)$$

where:
L_{FP}: design length of the cavity
$L_{\tau_{back,frnt}}$: Phase penetration depth in the back(front) mirror
$\tau_{r(back,frnt)}$: reflection delay for the back(front) mirror

...and k is an integer. Note, if the cavity length is designed to the same center frequency as the DBR mirrors, the penetration depth and reflection delay terms cancel, so the penetration into the mirrors does not affect the designed resonant mode of the laser. Dispersion will affect the mode *spacing*, however. The penetration will be affected by dispersion, since the change in refractive indices of the layers alters Δn. This will alter the longitudinal mode spacing.

Mirror Losses Normally the mirror losses for the VCSEL are accounted for by the penetration depth and the expected loss coefficient for the material (α_m). The energy penetration depth is usually used for this purpose. Babic and Corzine have shown [4] that for large numbers of layers ($m > 8$) the phase and energy penetration depths approximate each other. For most VCSEL mirror applications, the design will exceed this constraint; hence one can use the phase penetration depth as the mirror penetration depth:

$$l_m = L_\tau = \frac{\tanh \kappa l}{2\kappa} \qquad (2.48)$$

...with $\kappa = 2\Delta n/\lambda_0$ as defined above.

III. Application and Performance

3.1 Introduction

The application of the equations developed in chapter 2 to the building of a vertical cavity structure is the aim of this chapter. Along the way, the equations in chapter II will allow the prediction of performance in the VCSELs to be grown. The initial designs for this effort focus on optically pumped VCSEL structures. Electrical stimulation of the active region is a longer range goal in this process. A summary of the options available for electrically stimulated VCSELs is included at the end of this chapter.

3.2 MQW InGaAs 950 nm Vertical Cavity Laser

The primary constraints on the cavity design for this thesis were the lasing wavelength (950 nm) and the mirror/cavity materials. The materials used were $In_x Ga_{1-x} As$ for the quantum wells, $Al_x Ga_{1-x} As$ for the spacers, barriers, and mirror layers. The choice of materials was dictated by the available materials (and number of cells) for the MBE growth. For AlGaAs quantum well VCSELs, an additional aluminum cell would have been required to grow two different Aluminum concentrations for the mirror layers. Rather than reconfigure to grow AlGaAs quantum well VCSELs, we decided to pursue InGaAs designs. These would allow the mirrors to be constructed of AlAs (low refractive index layers) and GaAs (high refractive index layers). The chosen VCSEL wavelength was 950 nm, but initial back mirror growths were designed for 920 nm; this choice was dictated by the available monochromator (max detectable wavelength: 926 nm). The later availability of a higher range monochromator prompted the decision to pursue a 950 nm VCSEL, along with the success of higher wavelength InGaAs cavities at the University of Arizona [17] and elsewhere [20], [16], [8]. The paragraphs below summarize the design process used to construct the VCSELs for this effort.

3.2.1 Active Medium
The material characteristics for $In_x Ga_{1-x} As$ vary with x-concentration. For quantum well designs, the transition energy, and as a result, the wavelength of the emissions, can vary with the band gap, the effective masses of the holes and

electrons, and the well width (see equation 2.31). Many combinations of these parameters can produce the desired lasing wavelength.

3.2.2 **InGaAs Active Region Parameters** For $In_x Ga_{1-x} As$ on a GaAs substrate, equations for the energy gap and the effective masses of the electrons and holes are [22]:

$$m_c^* \Rightarrow m_e(x) \quad = \quad [.0665 - 0.0435x]\, m_0 \tag{3.1}$$

$$m_v \Rightarrow m_{hh}(x) \quad = \quad [0.45 - 0.04x]\, m_0 \tag{3.2}$$

...where m_0 is the free electron mass. No light-hole effective mass equations were available, but this should not affect the estimate greatly. InGaAs quantum wells on GaAs substrates undergo only compressive strain [12], which favors the heavy hole transition. The band gap energy for bulk $In_x Ga_{1-x} As$ at T=300K is:

$$E_G(x) = 1.424 - 1.614x + 0.54x^2 \quad \text{eV} \tag{3.3}$$

For threshold current minimization, the material gain at 950 nm as a function of x concentration should be determined. The most rigorous procedure would be to plot the spectral gain equation [32]:

$$g(E) = \left(\frac{\pi e^2 \hbar}{\epsilon_0 n c m_0^2 E} \right) |M|^2 \rho_{red}(E)(f_c - f_v) \tag{3.4}$$

where:
$g(E)$: spectral gain
m_0: free electron mass
n: index of refraction
ϵ_0: permittivity of free space
c: speed of light (vacuum)
$|M|$: momentum matrix element for the region
ρ_{red}: reduced density of states
$f_{c,v}$: Probability band state is occupied

The use of this equation would provide the material gain for a particular frequency ($E = h\nu$) which could be plotted vs x-concentration to determine the concentration that gives the maximum material gain. To do so it is necessary to know, for x-concentrations, the electron and hole effective masses (m_c^*, m_v), the bulk material energy gap (E_G), the spin orbit split-off energy (Δ_0), and the energy dispersion of the conduction band (m^*). These parameters have been determined for x-concentrations for $Al_xGa_{1-x}As$ on a GaAs substrate [2] and $In_xGa_{1-x}As_yP_{1-y}$ on an InP substrate [1], [24], but not all have been developed for $In_xGa_{1-x}As$ on a GaAs substrate. Even without these parameters, we can still make an informed choice for the Indium (x) concentration.

Since the quantum well barriers should be a close lattice match to the active region, it is a natural choice to use GaAs for the barriers, which provides a close lattice match to the InGaAs in the quantum wells. An added benefit of choosing GaAs for the barriers is that superlattices with GaAs layers have evidenced a tendency to produce very good layer uniformity in other VCSEL growth reports [14]. As noted in chapter 2 the barriers should be at least 100 Å to avoid interwell coupling. With the considerations above, we will use 100 Å thick GaAs barriers, which have a bulk band gap of 1.424 eV at room temperature [2].

3.2.3 **Well Width and x Concentration** Now, turning to the transition energy equation (from eq 2.31):

$$h\nu = E_G(x) + \left(\frac{1}{m_c^*(x)} + \frac{1}{m_v(x)}\right)\frac{\hbar^2}{2}\left(k^2 + l^2\frac{\pi^2}{L_z^2}\right)$$

Selection Rules Yariv notes that since the l=1 states in the conduction and valence bands have the highest populations, the highest optical gain is to be obtained from the $l = 1(k = 0)$ conduction-to-valence band transition (maximizes ($f_c - f_v$) in equation 3.4 above). The transition energy equation then reduces to:

$$h\nu = E_G(x) + \left(\frac{1}{m_c^*(x)} + \frac{1}{m_v(x)}\right)\frac{\hbar^2}{2}\left(\frac{\pi^2}{L_z^2}\right) \qquad \{\, l = 1, k = 0\,\} \qquad (3.5)$$

A plot of the equation above for $\lambda = 950$ nm is at figure 3.1.
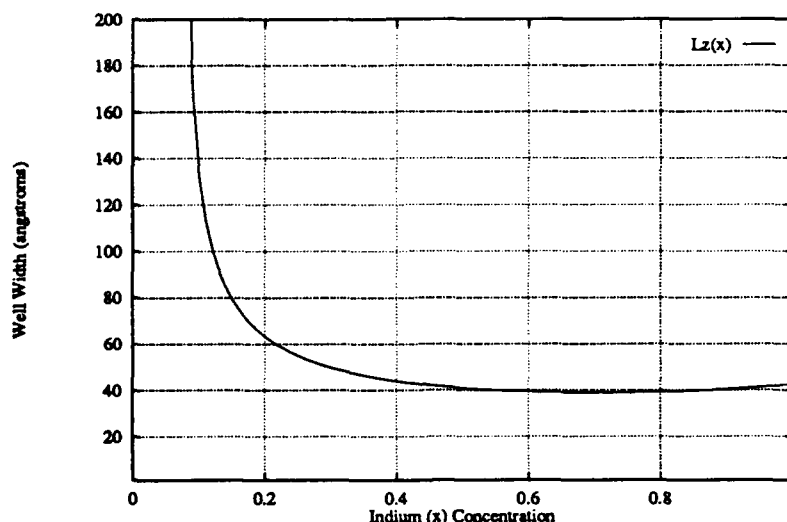
Figure 3.1. Required Quantum Well Width vs Indium Concentration for $\lambda = 950$ nm (l=1, k=0)

The x concentration chosen for this VCSEL is $x = .2$, corresponding to a 64 Åwell width. In choosing this well width it is necessary to consider not just the transition energy:

- Barrier Height: This width provides the necessary barrier height: the bulk energy gap for the $x = .2$ concentration, using equation 3.3, is 1.123 eV. Corzine recommends the well-barrier height at the conduction band edge be at least 100 mev [11] to preserve the energy quantization. Kolbas [22] says the conduction/valence band split is 70/30 for InGaAs on GaAs. The gap for GaAs (1.424 eV) should, then, be large enough to provide the necessary well-barrier height $(.7 \times (1.424 - 1.123) = 210 mev)$.

- Critical Thickness: The 64 Åwell widths should be safely below the critical thickness [15], even for multiple wells [20]. The barriers will be 100 Åwide to preclude interwell coupling, and this is also below the critical thickness.

- Fabrication Capability: The 64 Åwell is within the capabilities of most MBE systems.

3.2.4 **Cavity Construction** Now that the active region's parameters are set, the periodic gain structure for the cavity may be determined. Cavity length is determined by the lasing wavelength and the number of active regions to be included. For this first-build, to limit growth time and complications, I limited the number of quantum wells to three. Additionally, three active regions were chosen for the PGS structure. Each active region having three quantum wells results in an optical thickness per region:

$$t_{act} = [3 \times 6.4 \times n_{act} + 2 \times 10 n_{barr}] \, nm$$

With $n_{barr} = 3.5455$ the index of refraction for GaAs at 950 nm using equation 2.42 outlined on page 2-23. A literature search turned up no ready means of determining the index of refraction for varying x-content in $In_x Ga_{1-x}As$. Fortunately, the refractive index of InAs is very close to that of GaAs (at 885 nm $n_{InAs} = 3.696$ and $n_{GaAs} = 3.633$). To estimate the index for $In_{0.2}Ga_{0.8}As$ we interpolate between these values to obtain $n_{act} = 3.5681$. These indices and the desired well and barrier thicknesses correspond to an optical thickness $t_{act} = 139.4 \, nm$. For the PGS with three active regions, the total optical thickness is $d \approx 418.25 \, nm$. The cavity was to be designed for a longitudinal mode of 950 nm. If the mirrors are designed for a center (Bragg) frequency at 950 nm, we can eliminate the penetration depth and reflection delay terms, as discussed in the *Mirror Design* section of Chapter II, and the cavity optical length can be determined from equation 2.47:

$$2\beta L_{FP} = 2\pi k$$

Here, $\beta = 2\pi/\lambda_0$, L_{FP} is the optical length of the cavity, and $k = 4$, since we want the longitudinal mode to peak at each of the active regions (see figure 3.2). As a result, the cavity should be two times the lasing wavelength or a $l = 1.9 \mu m$ optical thickness. This corresponds to a fill factor d/l of .22. Corzine recommends fill factors in the vicinity of 0.2 - 0.3 for optimal confinement factors [11].

The logical choice for the spacers is GaAs, since it lattice matches well to both the InGaAs wells and the AlGaAs mirror layers adjacent to the cavity, and provides a band

3-5

gap sufficiently removed from the active region band gap to minimize absorption. For the parameters discussed so far, with $t_{act} = 139.4$ nm and $\lambda/2 = 475$ nm, the spacer should be 335.58 nm optical thickness. Since the spacer is GaAs ($n = 3.546$) the physical thickness of the spacer is $335.58/3.546 = 94.65$ nm. Now, placing the active regions at the peaks of the electromagnetic mode, the cavity takes the form of figure 3.2. The spacers adjacent to the mirrors have been lengthened so that the three active regions, two interior spacers, and 2 outside spacers, combine for a total cavity optical length of 2 λ.
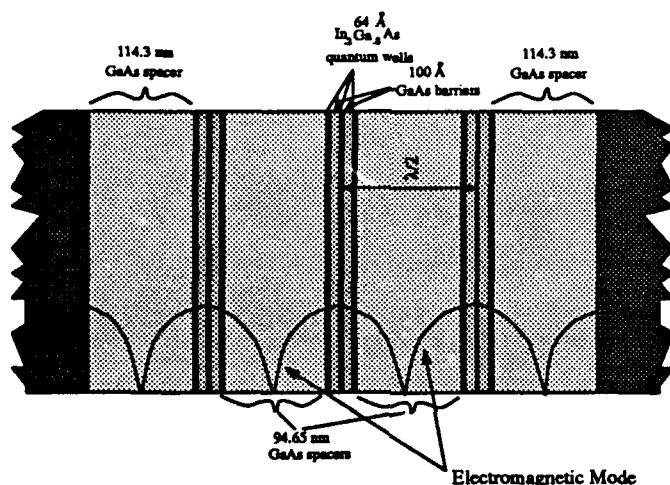
Figure 3.2. Cavity for the $In_{0.2}Ga_{0.8}As$/GaAs 64 ÅQuantum Well VCSEL

3.2.5 **Mirror Design** The mirrors for the cavity design from the previous section were designed with a Bragg frequency of 950 nm. The use of InGaAs for the active regions allows the use of GaAs in the mirrors, since the higher band gap of the GaAs mirror layers will make it a low loss material at the lasing wavelength. The mirrors were constructed of $Al_xGa_{1-x}As$; this allowed uninterrupted growth for the MBE fabrication. The natural choice for the concentrations is AlAs/GaAs. This combination provides the greatest refractive index difference for the $Al_xGa_{1-x}As$ family. Large Δn is important, as the number of layers required to reach a desired reflectivity decreases as Δn goes up. The VCSEL will be grown on a GaAs substrate to provide adequate lattice matching for the mirror layers.

920 nm Bragg Frequency Mirror Design   The initial back mirror was grown to be testable with the reflectivity measurement systems available. At 920 nm center frequency, the transmission matrix approach outlined in Chapter 2 indicates a reflectivity of 99.17 % can be achieved for the mirror with 17 periods of AlAs/GaAs pairs, starting with AlAs and ending with GaAs. The parameters for the mirror are below, followed by a calculated reflectivity curve in figure 3.3, produced via the FORTRAN program DBR.f included in Appendix A.

Number of Layers:	34
Substrate:	GaAs
Peak Reflectivity:	99.14 % @ 920 nm in air
Low Index Layers:	AlAs
Calculated Index:	2.98151
Physical Layer width:	77.1 nm
High Index Layers:	GaAs
Calculated Index:	3.5727
Physical Layer width:	64.3 nm
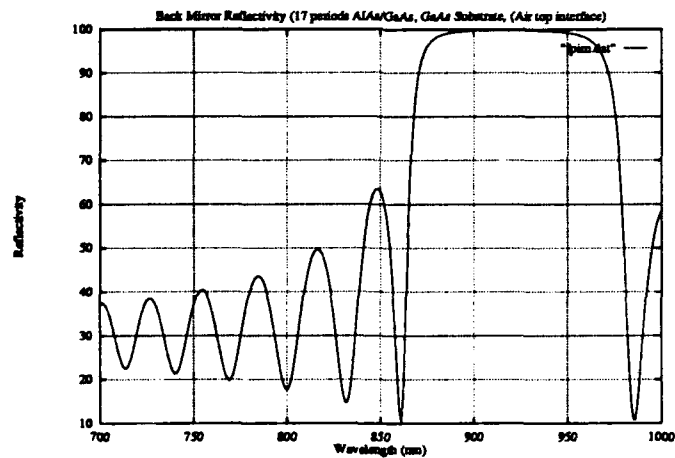
Figure 3.3. Bottom Mirror Reflectivity as seen in Air

950 nm Bragg Frequency Mirror Design   The back mirror for the final VCSEL structure will be grown for a Bragg frequency of 950 nm. At 950 nm center frequency the transmission matrix approach outlined in Chapter 2 indicates a reflectivity of 99.6 % can be achieved in the GaAs spacer with 19 1/2 periods of AlAs/GaAs pairs,

starting with AlAs and ending with AlAs. The parameters for the mirror are below, followed by a calculated reflectivity curve for the structure as seen in the GaAs spacer (figure 3.4), produced via the FORTRAN program DBR.f included in Appendix A.

Number of Layers:	39
Substrate:	GaAs
Peak Reflectivity:	99.6 % @ 950 nm in GaAs
Low Index Layers:	AlAs
Calculated Index:	2.9742
Physical Layer width:	79.85 nm
High Index Layers:	GaAs
Calculated Index:	3.5455
Physical Layer width:	66.99 nm
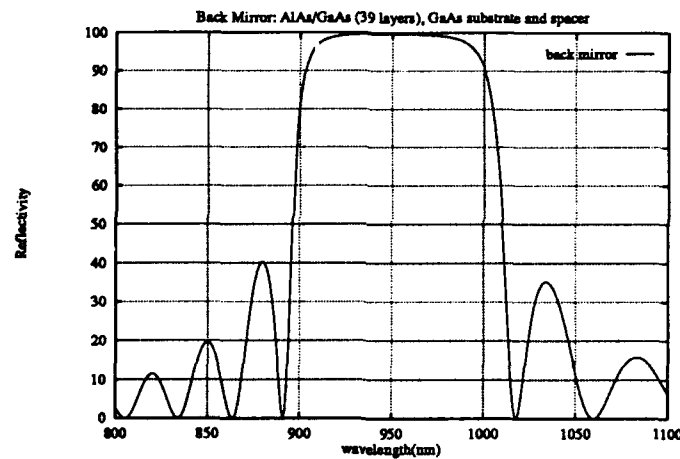
Figure 3.4. Bottom Mirror Reflectivity as seen in GaAs Spacer

Top Mirror Design The VCSELs to be designed for this thesis were to have the output beam exiting via the top of the wafer. With this in consideration, the bottom mirror design is straightforward; it requires only a high reflectivity and low loss. The top mirror, however, must provide enough reflectivity to satisfy the threshold gain equation (equation 2.3), *and* provide a low enough reflectivity to favor the beam exiting the top mirror. Most successful designs have resulted after several iterations of fabrication and measurements. The measurements provide an accurate means of determining the gain/loss profiles of the materials to be used in the VCSEL design. For a first cut, Corzine

3-8

[11] has achieved success with a geometric mean reflectivity for the mirrors of > 95 %. This reflectivity is on the order of those used in successful designs at the University of Arizona [17], and at AT&T [19]. Given the bottom mirror reflectivity (99.6 %) and this minimum geometric mean, the top mirror must exceed 91 % reflectivity. To provide a margin of assurance, I chose a reflectivity of 97 %. This top mirror reflectivity provides an overall geometric mean reflectivity of:

$$R = \sqrt{R_{btm}R_{top}} = \sqrt{.996 \times .97}$$
$$= 98.3\%$$

To provide the top mirror reflectivity, the design must achieve the 97 % goal with the incident medium being GaAs and the exiting medium air. Since the spacer is GaAs, the first layer of the GaAs/AlAs top mirror should be AlAs, (a GaAs first layer next to the spacer provides no added reflection). The top layer should be GaAs, since it provides a larger index difference with the air interface, and GaAs is less prone to oxidation. As a result, we will have an even number of layers in the top mirror. To determine the number of layers, we use equation 2.41 to get the admittance Y. At normal incidence $\mu_0 = n_0$; we are interested in the reflectivity from the spacer looking out, $n_0 = n_{GaAs} \approx 3.5455$, $n_{sub} = n_{air} \approx 1.0$ at the 950 nm center wavelength:

$$\Re = \left| \frac{\mu_0 - Y}{\mu_0 + Y} \right|^2$$
$$\Rightarrow \pm\sqrt{.97} = \frac{n_{GaAs} - Y}{n_{GaAs} + Y}$$
$$\Rightarrow Y = .0269$$

With this admittance Y, and knowing we need an even number of layers N, we can use equation 2.40, with the indices of refraction for GaAs and AlAs at normal incidence to determine N.

$$Y = \frac{\mu_1^2 \mu_3^2 \dots \mu_{N-1}^2 \mu_{sub}}{\mu_2^2 \mu_4^2 \dots \mu_N^2}$$
$$\Rightarrow Y = \frac{n_{AlAs}^N n_0}{n_{GaAs}^N}$$

$$\Rightarrow \quad .0269 = \frac{2.9742^N 1.0}{3.5455^N}$$

$$\Rightarrow \quad N = 20.6$$
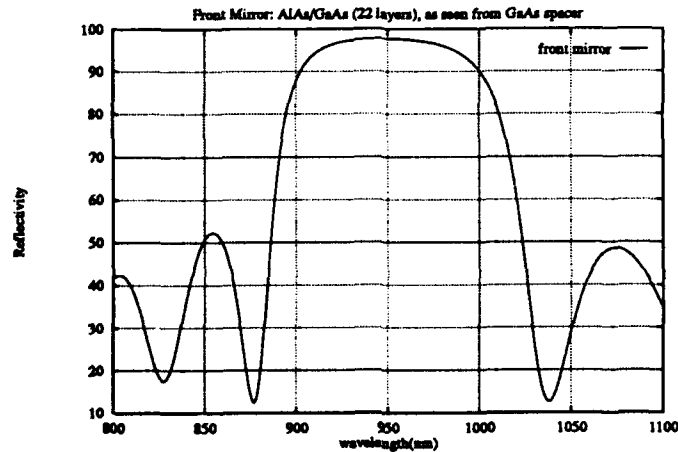
Figure 3.5. Top Mirror (22 layers) Reflectivity as seen from GaAs Cavity Spacer

To exceed the 97 % goal, we choose N to be 22. The reflectivity curve for the top mirror, as seen from the GaAs spacer is plotted in figure 3.5.

The overall reflectivity of the VCSEL is plotted in figure 3.6. The structure has a stop band of 125 nm about the 950 nm center frequency. The Fabry Perot resonance is at 950 nm. The closest minimum is at 883 nm, this is the likely wavelength location for the pumping laser. The maximum reflectivity is approximately 99.98 %; air being the incident medium. Neglecting dispersion for a moment, by solving equation 2.47 for $k = 3$ and $k = 5$ the nearest neighboring modes to the 950 nm resonant frequency would be 1019 nm and 890 nm. Both modes will have a significantly lower gain as compared to the 950 nm longitudinal mode and both have significantly lower reflectivity, falling at the edges of the stop band. These factors conspire to prevent lasing of these neighboring longitudinal modes.
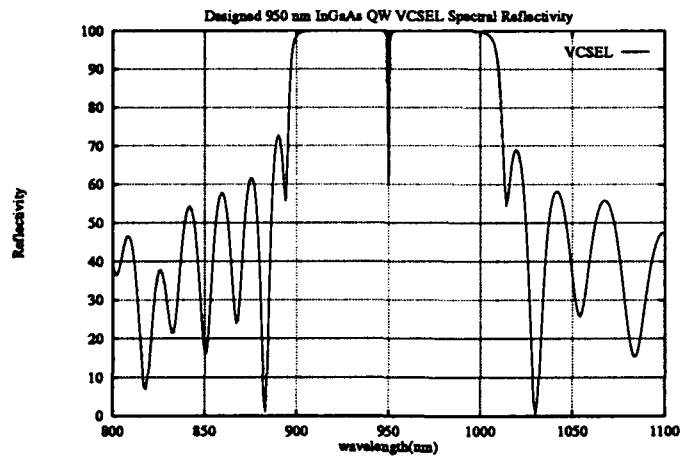
Figure 3.6. Fabry-Perot Effect in Designed 950 nm VCSEL using 39 layers AlAs/GaAs bottom mirror and 22 GaAs/AlAs layers (top) with 2 λ MQW spacer

3.3 Carrier Guided VCSELs

The VCSELs measured in this research were not processed further after their MBE growth. It is common to impart a mechanism to provide a means of guiding the carriers which will be optically, or electrically, injected. Gain guiding and index guiding are the typical choices.
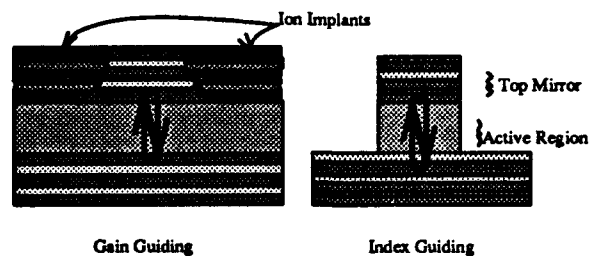
Figure 3.7. Gain Guiding and Index Guiding in Conventional Processed VCSEL Structures

Designed gain guiding is usually accomplished by ion implantation on the wafer (see figure 3.7). The ion implantation is achieved by conventional masking and implantation techniques [19]. Regions are formed in the wafer which inhibit gain in volumes adjacent to the volume where lasing is desired. The relatively high gain region tends to concentrate

the carrier population in the desired volume, favoring stimulated emission. Index guiding is less subtle. By etching the mirror and cavity layers away from the substrate to form a columnar structure, the air/semiconductor index difference at the sides of the column is used to contain the carriers.

The VCSELs tested for this effort did not use ion implantation or etching to provide a guide mechanism for the carriers. With sufficient pump power and a small enough pump spot, the optically generated carriers can form their own guide mechanisms. The injection of the carriers tends to elevate the gain in the area around the pump spot; in addition, the high concentration of carriers also tends to increase the local refractive index of the medium. Thus, the carriers form a self generated gain and index guiding mechanism to favor the population inversion [13]. This type of carrier induced guiding is illustrated in figure 3.8.

Carrier Generated Gain/Index Guiding
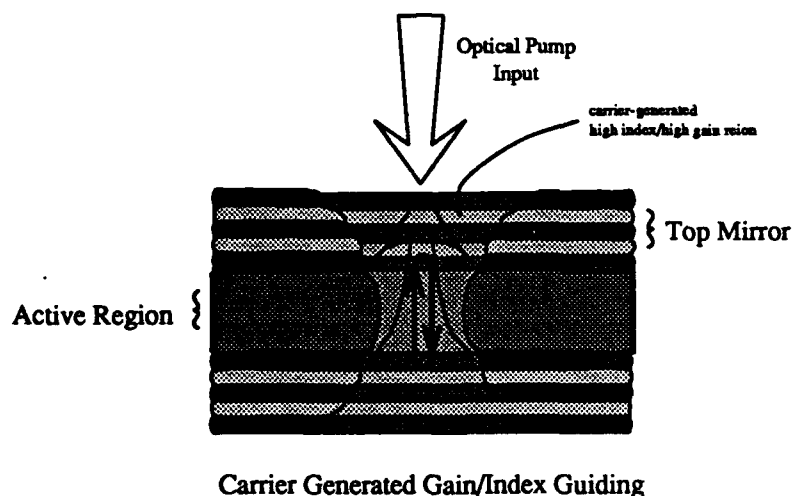
Figure 3.8. Gain and Index Guiding from Carrier Injection

3.4 Injection Lasers: Electrical Pumping

The design so far has focused on the building of optically pumped surface emitters. The formation of a junction in the VCSEL doesn't present much difficulty, the entire structure is of semiconductor and it is relatively straightforward to impart dopants to the layers as necessary to form the desired acceptor/donor levels. A p-i-n structure is the

commonly used scheme, leaving the active region undoped to lower cavity losses [19]. The difficulty in electrical injection is that the same abrupt discontinuities in the mirror layers that provide efficient DBR reflection result in high resistivity of the structure. As with other advances in VCSEL design, the lead of in-plane semiconductor lasers provided a guide for early VCSEL designs in this area.

3.4.1 **Active Region Design** A natural improvement to the abrupt well-barrier structure of the quantum wells used for this thesis is the Graded Index Separate Confinement Heterostructure (GRIN SCH). The GRIN SCH employs a superlattice at the well-barrier interface to provide a smoother transition from the well to the barrier. The separate confinement heterostructure increases the confinement factor (Γ), which falls off as the square of the thickness of the active region ($\sim t^2$) [32]. As the quantum wells become thinner, the reduction in Γ can become significant. The GRIN SCH is more effective than abrupt interfaces at capturing carriers in the wells. This becomes important for thin quantum wells.

There is a residual benefit of this structure for current injection purposes. The gradual variations in the energy gap (compared to those for abrupt interfaces) between materials provide less dramatic well/barrier discontinuities. This lowers resistance of the structure [19]. Non-quantum well structures can also use graded index interfaces to reduce resistances in the active regions. The application is a straightforward extension of that used in the injection design for the DBR mirrors described below. The number of interfaces to be concerned about in either UGS or PGS active regions is relatively few compared to the DBR mirrors. As a result, the pay back for the design effort is less dramatic.

3.4.2 **DBR Mirror Design** The abrupt discontinuities of the DBR mirror as described for the optically pumped structures of this thesis will provide relatively high resistivities if used in an injection scheme. In the p-type layers, the periodic well-barrier discontinuities produce the high resistances. In the n-type layers, the high resistance is attributed to poor conductivity of the AlAs layers [19].

The remedies to the resistance of the mirror layers include softening the energy gap transitions (non-abrupt interfaces) or etching through the mirrors to inject carriers directly, avoiding the discontinuities in the mirror layers. These two methods are shown in figure 3.9 below.

Non-Abrupt Interfaces (Superlattice)   Transverse Current Flow
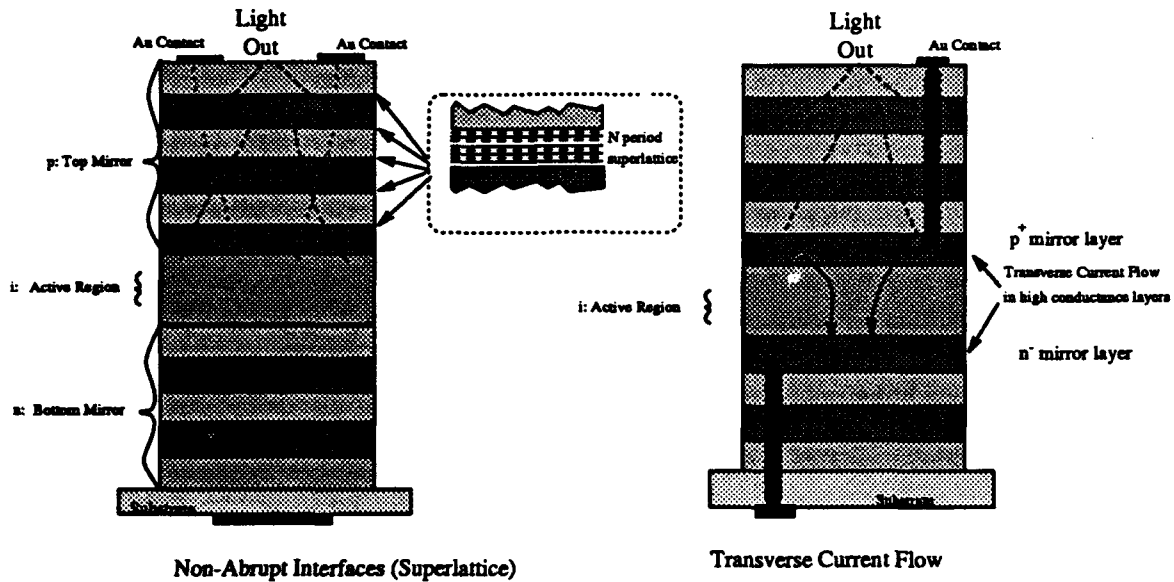
Figure 3.9. Two Methods of Avoiding High Mirror Layer Resistances for Current Injection in VCSELs

Non-Abrupt Interfaces The use of non-abrupt interfaces has met very good success. Two methods are prevalent. The first is to limit the x concentrations of the two mirror layers so that their difference is less than $\Delta x = 0.6$. This approach, however, increases light penetration into the mirrors, which will increase mirror loss, and require more layers to achieve a desired reflectivity.

The second method (which is shown in figure 3.9) is to incorporate superlattice transitions between the layers in the DBR mirrors. Tai achieved two orders-of-magnitude reduction in resistivity using a 10 Å, 10 period superlattice at each interface. The super lattice was $Al_{0.7}Ga_{0.3}As$ /GaAs and the quarter wave layers were also $Al_{0.7}Ga_{0.3}As$ /GaAs [31].

Transverse Current Flow   As a promising alternative to non-abrupt interfaces, Jewell suggests the use of a transverse current in high conducting layers above and below the active region. The current would be injected by etching through the mirrors to place contacts. This method stems from the power efficiency equation of the VCSEL structure, given by [19]:

$$P_{eff} = \eta_{eff} \times \frac{I_{op} - I_{th}}{I_{op}} \times \frac{V_g}{V_g + I_{op}R} \qquad (3.6)$$

where:
P_{eff}:	power efficiency
η_{eff}:	differential quantum efficiency
I_{op}:	operating current
I_{th}:	threshold current
V_g:	normalized bandgap energy
R:	series resistance of the VCSEL structure

This equation shows how an increased voltage drop ($I_{op}R$) lowers the power efficiency. To lower series resistance R, vertical, rather than transverse, current flow is desired through the active region. Transverse current flow through the undoped active region increases the voltage drop, which decreases efficiency. High conductivity layers would be used above and below the active region for transverse current flow, and current flow through the active region would then be vertical. The drawback of this structure is the extra processing required to produce the desired current flow. This extra processing is compounded as the packing density is increased.

IV. Experimental Method

The experimental part of this research involved measuring output beam character-
istics and surface reflectivities. All of the output beam characteristics and many of the
surface reflectivity measurements were performed using one experiment configuration. Ad-
ditional reflectivity measurements with an alternate configuration were performed to com-
pensate for some of the equipment limitations encountered in covering the wavelength
range for the InGaAs structures.

4.1 Laboratory Configuration

The equipment configuration used to optically pump the samples is shown in figure
4.1. In this configuration, the pump beam enters the VCSEL vertically via the top mirror.
A short focal length lens is used to concentrate the pump onto a small area of the structure
(see figure 4.2).
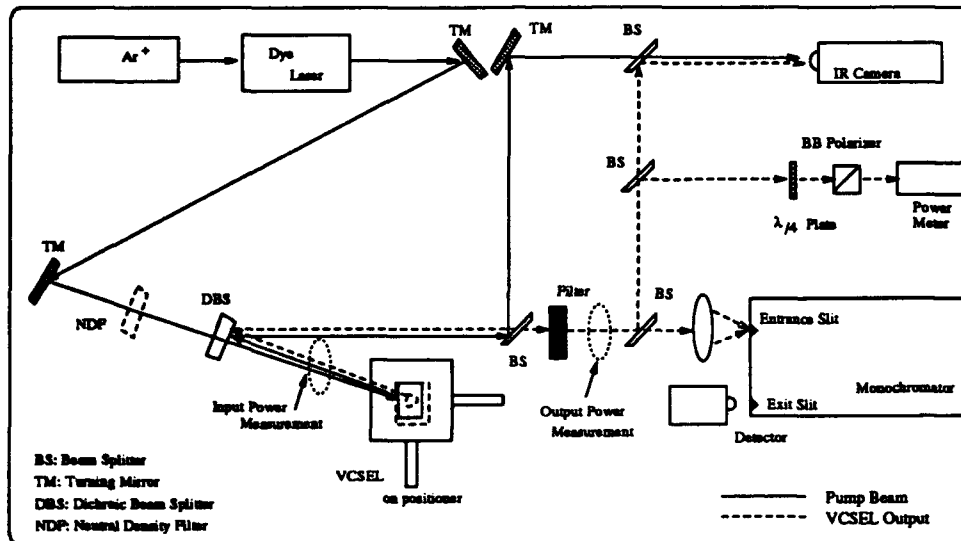
Figure 4.1. Equipment Configuration used for Output Beam Characterization

The output beam exits via the top of the wafer for all of the samples measured in this
experiment. The output beam travels back down the same optical path as the reflected
pump beam. The pump and output are then separated via filters and beamsplitters and

directed to the measurement devices. A brief description of the major elements in the configuration follows, Table 4.1 provides relevant specifications for the equipment:
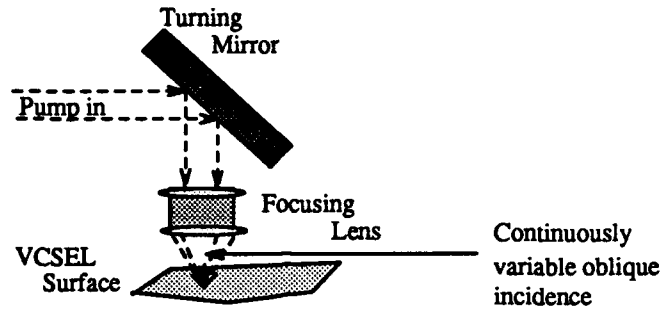
Figure 4.2. Optical Pump Beam and Focusing Lens Geometry

Ar⁺ Laser	Provides the means to optica.ly pump the dye laser. The Argon laser is the optical power source for the experiment
Dye Laser	Chosen to provide a tunable pumping source. The dye used for this application (LDS-821) provided a wavelength range (790 nm - 905 nm) which covered the typical pump wavelengths for both GaAs and InGaAs VCSELs. The tunable dye laser also provided a means of measuring the spectral reflectivity of the samples.
Dichroic Beamsplitter	The DBS used to pump the GaAs VCSELs had a maximum transmissivity at 830 nm and a maximum reflectivity at 870 nm. This property allowed the incident pump to pass from the dye laser. After reaching the sample, the output laser and the pump return to the DBS (see figure 4.1). The DBS transmits most of the pump and reflects most of the output beam. This provides part of the filtering of the pump from the VCSEL output.
Focusing Lens	Short focal length (8 mm) lens which focused the pump beam on the wafer.
Positioner	An accurate positioner was necessary to provide repeatable positioning of the pump onto the wafer surface.
Power Meter	used to measure pump power in, reflected power from the wafer, and VCSEL power out.
Filter	was used to filter the remainder of the reflected pump from the VCSEL output before allowing the VCSEL component to pass to the measurement devices.
TEC	The Thermoelectric cooler (TEC) was used to maintain constant temperature for the samples, which tended to heat from the incident pump energy. The TEC was mounted between copper plates. The bottom copper plate was attached to a heat sink which was later glued to the top of the positioner. The VCSEL was bonded with heat sink compound to the top copper plate. All surfaces between the VCSEL wafer and the heat sink were coated with heat sink compound to form thermal bonds.
Monochromator	The monochromator was used to determine the output wavelength of the VCSEL as well as the pump wavelength (when the narrowband filter is removed). A detector was used to monitor the exit slit of the monochromator.

IR Camera   The pump and VCSEL output were separately directed to the IR camera to image the spots from the top of the wafer. This allowed a measure of the laser spot diameter, by comparison to the size of the imaged pump spot. The minimum spot size for the focusing lens at the VCSEL provided the pump spot size. The image of the pump spot also allowed a qualitative assessment of the wafer surface.

Polarizer Cube   Used to determine the polarization of the output beam. Component polarizations were determined by inserting a quarter wave plate to rotate the light incident from the sample.

Table 4.1. Equipment Specifications for Laboratory Configuration

Ar^+ Laser	Model	Spectra-Physics 2020-03
	Wavelength	514.5 nm
	Output Power	$\sim 6W$
Dye Laser	Model	Spectra-Physics 375-50
	Dye	LDS-821 (Styril 9)
	Wavelength	Tunable 790 - 905 nm
	Output Power	~ 200 mW (typical)
	Linewidth	~ 666 Å
	Beam Divergence	1.6 mrad
	Beam Mode	TEM_{00} Vertically Polarized
	Mode Spacing	420 MHz
Dichroic Beam Splitter	Mfr	CVI
	R_{max}	870 nm
	T_{max}	830 nm at $\theta = 5°$
Filter	Mfr	Ealing
	Center Wavelength	880 nm
	BW (FWHM)	10 nm
Monochromator	Model	Ebert 82-546
	Wavelength Range	200 nm - 926 nm
	Accuracy	± 2 Å
Power Meter	Model	Coherent Fieldmaster
	Detector	LM-2 Silicon Sensor
Focusing Lens	Mfr	Melles Griot
	f_0	8 mm
	spot size	1.02 μm
	working distance	1.13 mm

4.1.1 **Dye Laser Configuration Reflectivity Measurements** Reflectivity measurements using the configuration in figure 4.1 were performed with and without the focusing lens. The lens provided a means of obtaining the reflectivity for a small spot on the wafer. This allowed reflectivity measurements for adjacent lasing and non-lasing spots to explore the link between reflectivity and lasing behavior. The reflectivities obtained with the lens in place are difficult to predict via the theory summarized in chapter II. The calculation is complicated by the action of the lens which focuses the collimated beam onto the spot (see figure 4.2). The light impinging on the spot is no longer normal to the surface. The pump rays are at varying degrees of oblique incidence, depending on where they enter the lens. The resultant reflectivity is a convolution of the obliquely incident ray reflectivities.

The lens measurements are more productive as a comparison from spot to spot on the wafer, rather than as a comparison to theoretical calculations. Additional measurements were done on the wafers without the focusing lens to compare measured to predicted reflectivity for orthogonal incidence. Measurements without the lens can provide a means of determining the quality of the fabrication of the wafer. For example, systematic thickness variations show as a shift in the reflectivity spectrum by changing δ_m in equation 2.34. A change in the Aluminum concentration of one of the layers will change the width of the stop band, as noted in section 2.4.4. The drawback to the measurements taken without the focusing lens is that the spot on the wafer is much larger ($\sim$ 3mm), so the reflectivity for the area is averaged over the area of the spot, which takes in both lasing and nonlasing locations.

4.1.2 **Additional Reflectivity Measurements** These measurements were performed to measure a broader spectral range than could be obtained from the measurement configuration in figure 4.1. The configuration is shown in figure 4.3, and consists of an Argon ion laser pumping a tunable Ti-Sapphire laser. The same power meter used for the dye laser measurements was used for these added reflectivity measurements. The Ti-Sapphire configuration provided a much broader measurement range (850 nm - 1.0 μm) for the reflectivity measurements.

These measurements were performed without a focusing lens for the incident beam, and represent the reflectivity for a broad ($\sim$ 3mm) spot on the wafer. To measure the reflected beam off the sample, the incident beam could not be orthogonal to the sample Oblique incidence shifts the reflectivity spectrally, as discussed in the *Mirror* section of chapter II. The measured reflectivities provided in chapter V are plotted against oblique incidence theoretical curves to compensate.
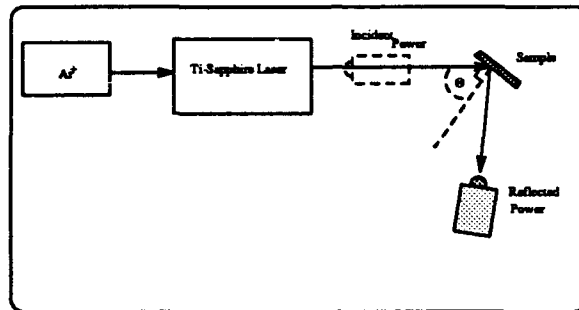

Figure 4.3. Additional Reflectivity Measurement Configuration

V. Experimental Results

The configuration described in chapter IV was used to measure characteristics from two VCSEL wafers with GaAs active regions. These samples were grown at the University of Arizona. Additionally, measurements on the back mirror for the VCSEL designed for this thesis were completed. Scheduling difficulties prevented completion of the full VCSEL structure designed in chapter III. The theoretical curves presented here are based on the theory outlined in chapters II and III, and used the programs in Appendix A to perform the calculations.

5.1 Measurement Parameters

The parameters measured for each sample were lasing wavelength, reflectivity, polarization, lasing mode, and pump wavelength.

5.1.1 Reflectivity
Each sample has a predicted reflectivity curve based on the growth parameters of the sample. These curves were calculated using the FORTRAN programs in Appendix A. Both lasing and non-lasing locations on the samples were measured for reflectivity vs wavelength. The measured wavelength range bracketed the upslope of the Fabry-Perot effect for the sample. Loss in the mirror and cavity layers due to absorption and scattering was not factored in for these curves. As a result, the theoretical spectral reflectivity curves can be much higher in magnitude than the measured curves.

The pump laser (dye laser) was attenuated to a level below that which would start VCSEL lasing; so that only surface reflectivity was collected. Input and output power were measured at the points indicated in figure 4.1. The reference reflectivity for the samples was a high reflectivity broadband mirror, substituted for the VCSEL sample. The designed reflectivity of this mirror was > 99.5 % over the wavelength range measured. The optical path for both the reference and the VCSEL sample included the turning mirror, focusing lens, and dichroic beamsplitter losses (see figures 4.1 and 4.2). The input to output power ratio for the VCSEL sample was then compared to this reference to determine the reflectivity of the sample.

5.1.2 Lasing Wavelength Lasing wavelength was measured using the monochromator indicated in Table 4.1. The wavelength accuracy of the monochromator was ± 2 Å.

5.1.3 Pump Wavelength Indicated the location of the pump that favored highest lasing output power. This characteristic was measured with the same monochromator used to measure the lasing wavelength.

5.1.4 Polarization The VCSELs measured in this research had GaAs bulk active regions (UGS). The close lattice match of these active regions to the $Al_xGa_{1-x}As$ mirror layers provides very little strain. As a result, random polarization was expected. The VCSEL samples used were small pieces of the original wafer with no growth directions indicated. Without a growth direction, the choice of which output polarization is horizontal, or vertical, is arbitrary. I chose to relate the polarization of the output of the VCSEL to the input pump from the dye laser. The dye laser output is vertically polarized (see table 4.1).The dye laser input polarization should not affect the VCSEL output polarization, since once the carriers are injected, stimulated emission in the GaAs active region forms its own polarization direction. The reflected dye laser pump, then, serves only as a convenient measurement reference for the VCSEL output polarization.

All polarizations measured were linear and in the same direction. Rotation of the dye laser pump beam polarization did not affect VCSEL output polarization. Since only four locations on each wafer were measured, it would be premature to draw conclusions concerning the polarization tendencies of these structures. The capability to measure the VCSEL output polarization, however, is now available for future studies with this configuration.

5.1.5 Mode A check on the lasing spot imaged in the infrared camera provided this measurement. When higher order transverse modes were encountered, input power and pump beam positioning were varied to see if they could alter the modes.

5.2 Sample 1: 3 λ UGS GaAs Active Region

Sample 1 consisted of a 3 λ long gain medium of GaAs, the 3 λ sample was the oldest sample used for this study; it was grown at the University of Arizona in November of 1990. The sample geometry is represented in figure 5.1 below, along with the locations on the surface where measurements were taken for lasing and non-lasing spots.
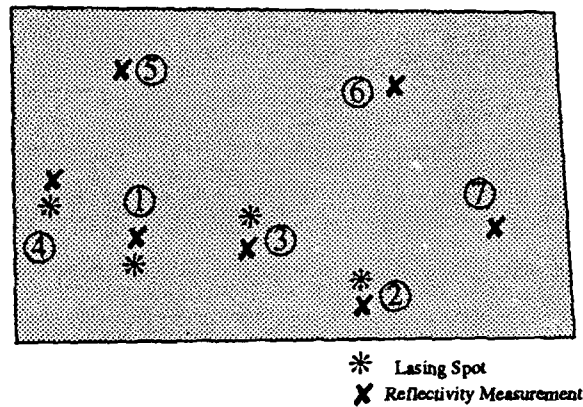
Figure 5.1. Sample 1: 3 λ Active Region VCSEL Geometry

5.2.1 Material Parameters
The material parameters for this sample are summarized below:

Number of Layers (front):	34
Number of Layers (back):	45
Active Region:	GaAs UGS
Active region thickness	.726 μm
Substrate:	GaAs
Design wavelength:	875 nm
Low Index Layers:	AlAs
Calculated Index @ 875 nm:	2.99573
Physical Layer width:	73.2 nm
High Index Layers:	$Al_{.127}Ga_{.873}As$
Calculated Index @ 875 nm:	3.52773
Physical Layer width:	61.8 nm

The theoretical reflectivity of Sample 1 based on the parameters described above (with no loss assumed) is represented in figure 5.2. There is a slight dip in the curve at

the design wavelength for the structure, due to the Fabry-Perot effect of the mirror/spacer integrated etalon. The minimum nearest the stop band is at $\approx 830nm$
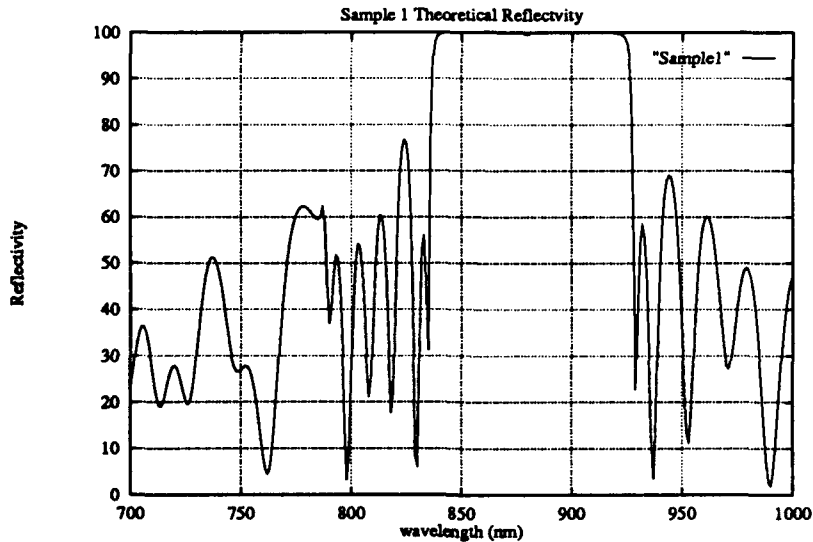
Figure 5.2. Sample 1: Theoretical Spectral Reflectivity near 875 nm

5.2.2 Sample 1 Measurements As shown in figure 5.1, lasing spots for sample 1 were grouped in the lower left quadrant of the sample. Reflectivity measurements for two of the spots, and output beam measurements for all of the lasing spots follow. The reflectivity measurements for two lasing spots are paired with reflectivity measurements for neighboring non-lasing spots. Additional reflectivity measurements at non lasing areas on the sample are also included.

Sample 1; Spot 1 :

Lasing Wavelength	872.0 nm
Pump Wavelength	833.0 nm
Polarization:	Horizontal
Mode:	TEM$_{00}$

Reflectivity The reflectivities measured for spot 1 indicate that the lasing and neighboring non-lasing areas on the wafer surface have very nearly the same

reflectivities. This indicates that the Aluminum concentrations and layer thicknesses are fairly uniform. These reflectivities represent a convolution of oblique incidence beams, the result of the use of the focusing lens (see figure 4.2) to pump the VCSEL. The location of the pump minimum at 833 nm indicates the structure has a reflectivity near the design minimum. Oblique incidence shifts the spectral reflectivity to shorter wavelengths; the lens convolves the incident beams to average the total shift. This indicates the structure may have slightly thicker mirror or spacer layers than designed.

The measured reflectivities do not reach the 99 % mark expected for the lower wavelengths of the stop band. Absorption and scattering losses, which were neglected in the calculated spectral reflectivity curve, contribute to the lower reflectivity.
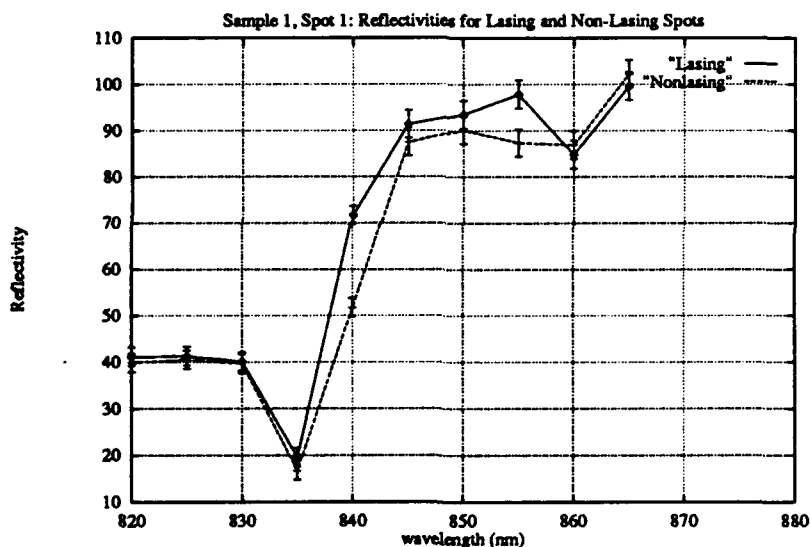
Figure 5.3. Sample 1 Measured Spectral Reflectivities for Lasing and Non-Lasing Locations near Spot 1

Sample 1; Spot 2 :

Lasing Wavelength	872.1 nm
Pump Wavelength	830.9 nm
Polarization:	Horizontal
Mode:	TEM_{00}

Reflectivity The reflectivities measured for spot 2 are also very similar from the lasing to non-lasing areas. The lasing spot's reflectivity curve in this case is distinctly higher at the longer wavelengths. The first minimum, however is nearly the same magnitude as for the non-lasing spot.

The difference in reflectivities for the wavelengths in the stop band are greater for spot 2. In all of the lasing/non-lasing areas, the imaged surface of the VCSEL wafer at 830 nm indicated a small ($\sim 1 \mu m$ as compared to the pump spot) 'island' on the wafer. When the pump spot was focused on this 'island', lasing would occur; movement of the pump off the 'island' ceased lasing. The effect could not be captured (photographed) with the configuration used for this experiment. The ability to see (in the imaged spot) the physical difference indicated there might be a change in reflectivities of the two areas. In some (such as spot 2 here) the difference in reflectivity was more dramatic.
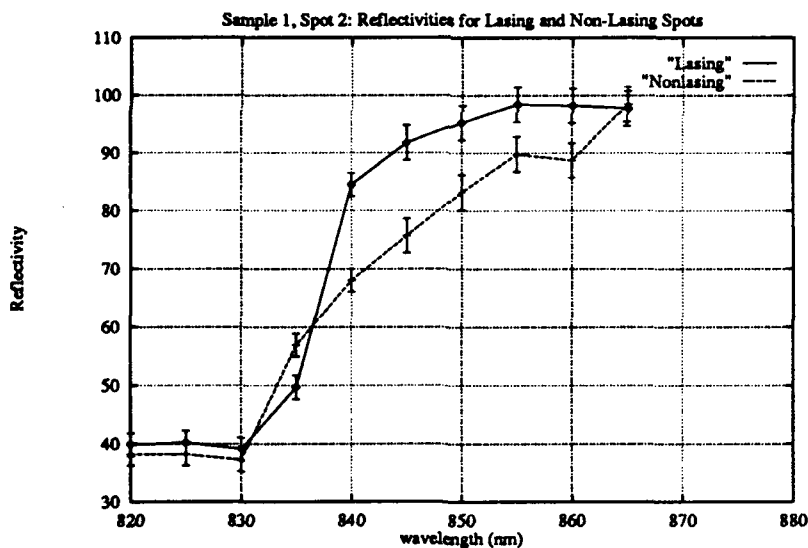

Figure 5.4. Sample 1 Measured Spectral Reflectivities for Lasing and Non-Lasing Locations near Spot 2

Sample 1; Spot 3 and Spot 4 Only lasing data are presented for Spot 3 and 4, as the reflectivity data for these spots is similar to that for Spots 1 and 2, and is not necessary for the subsequent analysis.

Spot 3:

Lasing Wavelength	874.1 nm
Pump Wavelength	832.0 nm
Polarization:	Horizontal
Mode:	TEM_{00}

Spot 4:

Lasing Wavelength	880.7 nm
Pump Wavelength	834.0 nm
Polarization:	Horizontal
Mode:	TEM_{00}

Sample 1; Non-Lasing Spots : Spots 5, 6 and 7 in figure 5.1 did not lase. In fact, they were representative of the areas on the wafer which did not even start photoluminescence. The reflectivity data for these areas is contained below and is included to allow comparison to the lasing areas for Sample 1 already presented.
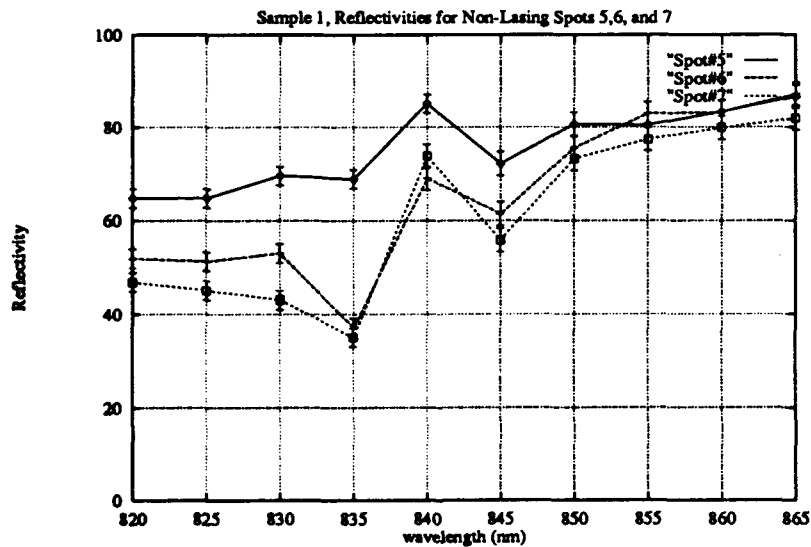
Figure 5.5.   Sample 1 Measured Spectral Reflectivity for Non-Lasing Locations: Spots 5, 6, and 7

5.2.3 **Sample 1 Analysis** The lasing wavelengths for this sample indicate the lasing behavior matched the design expectations fairly closely ($\lambda \approx 875nm$). Spots 1, 3, and 4 indicated pump locations near the first dip in the Fabry-Perot curve adjacent to the stop band. A slight shift to shorter wavelengths could be due to the oblique incidence forced by the focusing lens.

Polarization was linear for all measured lasing spots on the wafer. The polarization direction was the same for all spots. Jewell indicates in a 1989 study that polarization did not favor a particular direction for GaAs VCSELs [21]. The spots measured here indicate a possible tendency; however, larger samples, with more lasing spots, and more complete details about the growth directions are needed to draw conclusions concerning polarization.

The mode for all four spots on sample 1 was TEM_{00}. A picture captured from spot 1 is shown in figure 5.6. The pump spot shown is imaged. The pump spot was assumed to be the spot size for the diode laser lens used to focus the collimated dye laser beam. The specified spot size for collimated input for this lens is 1.02 μm (see table 4.1). This provides a measure of the spot size for the VCSEL output relative to the $\approx 1.02\mu m$ pump spot; the VCSEL spot, then is approximately 2.5 μm in diameter.

VCSEL Spot
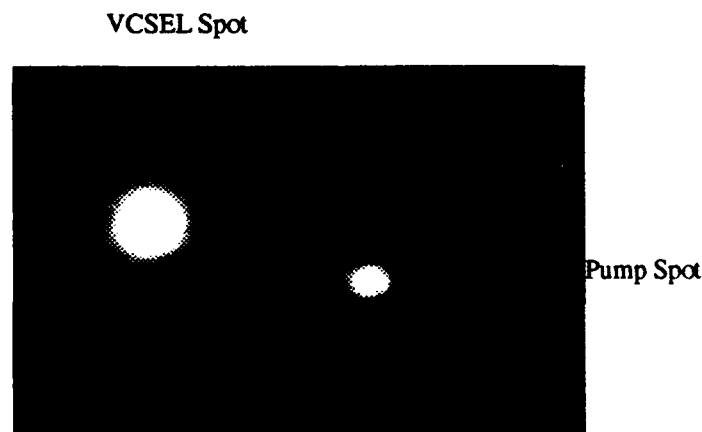
Figure 5.6. Sample 1, Spot 1 : TEM_{00} Lasing and Pump Spots

The reflectivity curves for each spot are nearly identical (see figure 5.3 and 5.4). With this close match, it is unlikely that spectral reflectivity alone can be used to predict

lasing behavior in VCSELs. Spots 5, 6, and 7, which were from an area of the VCSEL wafer which evidenced no tendency to lase, show low reflectivities where the stop band should be ($\approx 80\%$), indicating reflectivity measurements could be used as a cursory check on the wafer's tendency toward lasing. However, if pursuing a quick means of determining fabrication success, final conclusions about lasing quality and the abundance of lasing spots on the sample would require a more than reflectivity measurements.

5.3 Sample 2: 3 λ UGS GaAs Active Region

Sample 2 had a design wavelength similar to that of sample 1, but had a greater number of front and back mirror layers. The sample was grown at the University of Arizona in June of 1991. Locations of lasing and non-lasing spots measured are contained in figure 5.7 below.
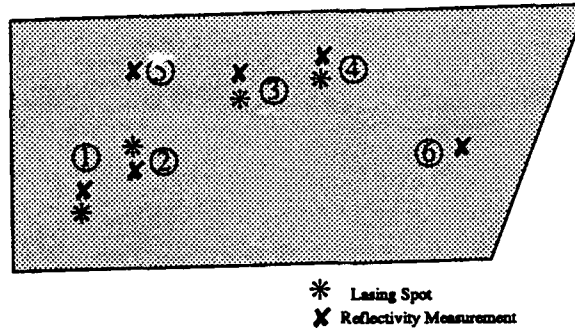
Figure 5.7. Sample 2: 3 λ Active Region VCSEL Geometry

5.3.1 Material Parameters
The material parameters for this sample are summarized below:

Number of Layers (front):	44
Number of Layers (back):	51
Active Region:	GaAs UGS
Active region thickness	.726 μm
Substrate:	GaAs
Design wavelength:	875 nm
Low Index Layers:	AlAs
Calculated Index @ 875 nm:	2.99573
Physical Layer width:	73.2 nm
High Index Layers:	$Al_{.127}Ga_{.873}As$
Calculated Index @ 875 nm:	3.52773
Physical Layer width:	61.8 nm

The calculated spectral reflectivity of Sample 2 based on the parameters described above (with no loss assumed) is represented in figure 5.8. The minimum nearest the stop band is at $\approx 824nm$

5-10
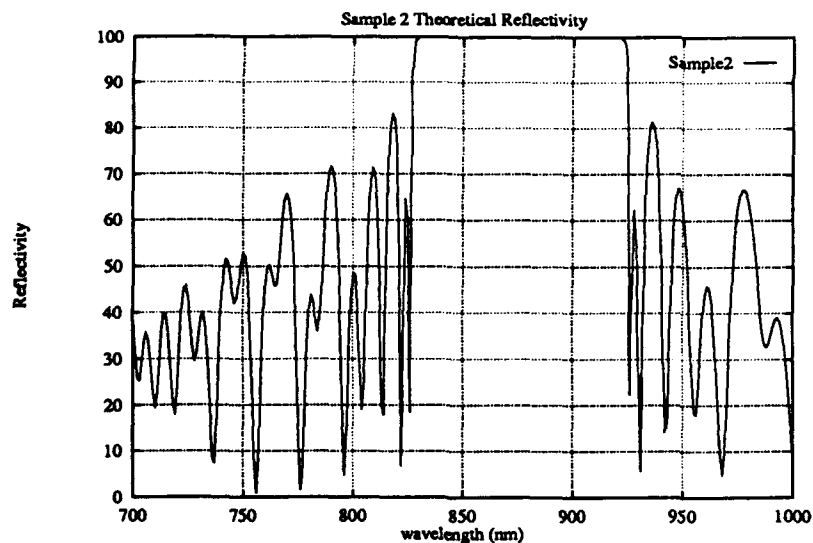
Figure 5.8. Sample 2: Theoretical Spectral Reflectivity near 875 nm

5.3.2 Sample 2 Measurements

Figure 5.7 shows the spots on sample 2 which evidenced lasing and non-lasing behavior. Again, reflectivity measurements were accomplished for all of these spots, but only those necessary for the analysis are included.

Sample 2; Spot 3 :

Lasing Wavelength	885.8 nm
Pump Wavelength	840.4 nm
Polarization:	Vertical
Mode:	TEM_{10}

Figure 5.9 is a reproduced image of the TEM_{10} mode this spot produced. The spot width is approximately 2.5 μm.

VCSEL Spot
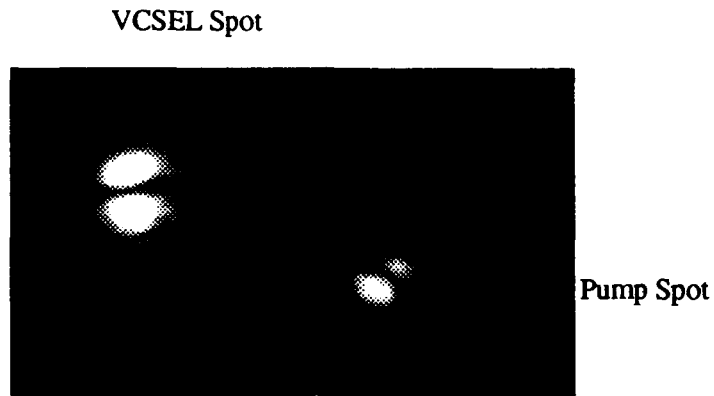
Figure 5.9. Sample 2, Spot 3: TEM_{10} Lasing and Pump Spots

Reflectivity As for sample 1, the reflectivities measured for sample 2, spot 3 indicate that the lasing and neighboring non-lasing areas on the wafer surface have very nearly the same reflectivities. Reflectivities for Sample 2 were collected every 2.5 nm to ensure minima in the curve were not bypassed.
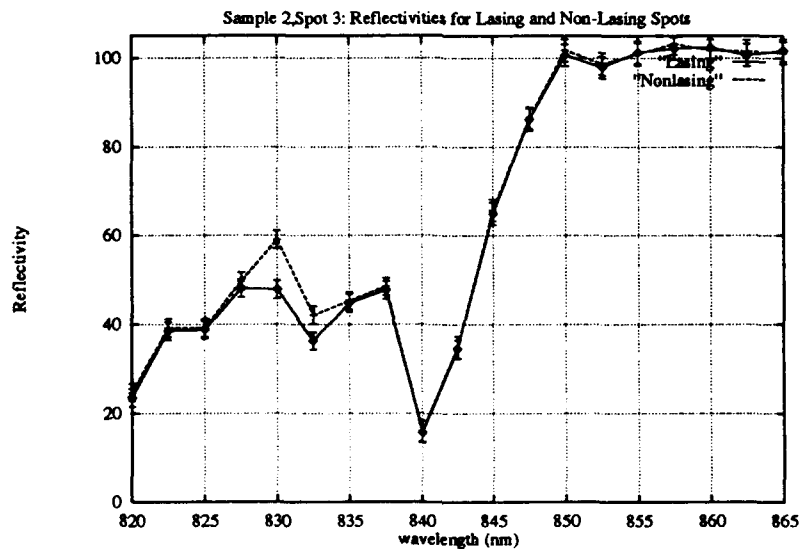
Figure 5.10. Sample 2 Measured Spectral Reflectivities for Lasing and Non-Lasing Locations near Spot 3

Sample 2; Spot 4 :

Lasing Wavelength	879.0 nm
Pump Wavelength	833.3 nm
Polarization:	Vertical
Mode:	TEM_{00}

Figure 5.11 shows the TEM_{00} mode this spot produced. The spot width is approximately 1.5 μm.

VCSEL Spot
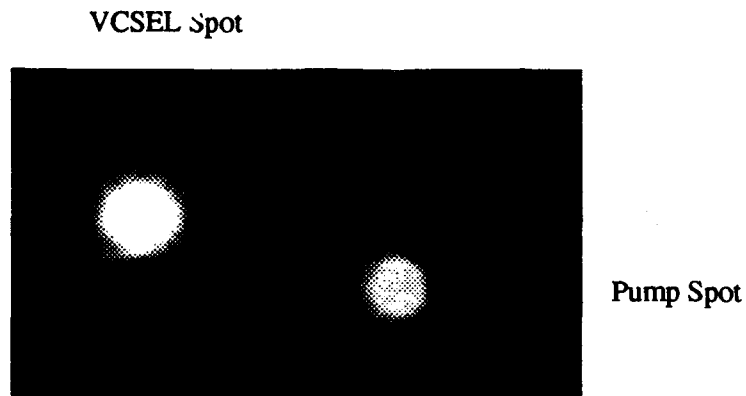
Pump Spot

Figure 5.11. Sample 2, Spot 4: TEM_{00} Lasing and Pump Spots

Reflectivity The spectral reflectivity for Spot 4 shown in figure 5.12 verifies the close reflectivity match shown for spot 3 of sample 2 above.

Sample 2; Spots 1 and 2 :

Spot1:

Lasing Wavelength	882.7 nm
Pump Wavelength	838.2 nm
Polarization:	Vertical
Mode:	TEM_{00}
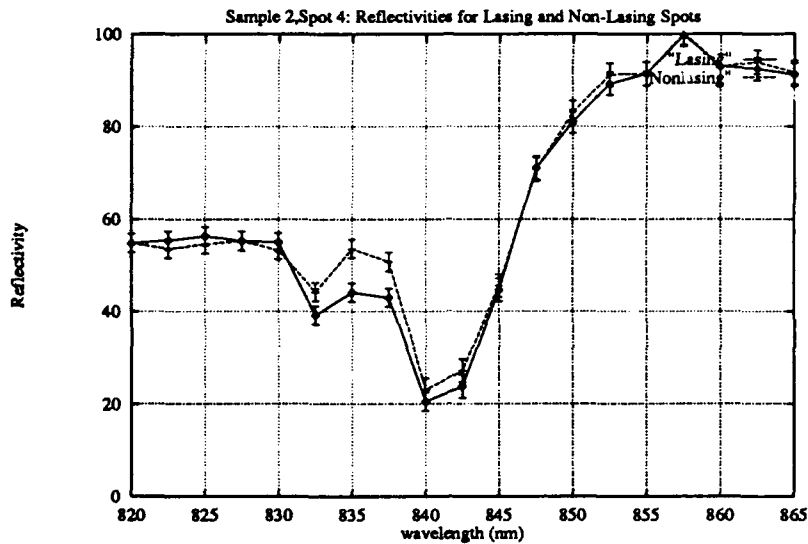
Figure 5.12. Sample 2 Measured Spectral Reflectivities for Lasing and Non-Lasing Locations near Spot 4

Spot 2:

Lasing Wavelength	880.5 nm
Pump Wavelength	835.8 nm
Polarization:	Vertical
Mode:	TEM_{00}

Sample 2; Non-Lasing Spots : Spots 5 and 6 in figure 5.7 did not lase. Reflectivities for these spots are included as representative of the non-lasing areas of sample 2. The reflectivity data for these areas is contained in figure 5.13.

Sample2: Reflectivity Measurements at Non-Oblique Incidence The measurements presented so far were performed with the focusing lens in place to allow reflectivity measurements of small spots on the surface of the wafers. To allow comparison to the theoretical reflectivity for normal incidence, the focusing lens was removed and the pump beam allowed to strike the surface of the wafer without interference. The resultant larger ($\sim$ 3mm) reflected spot forms an average reflectance over a larger area of the wafer. Two measurements were performed on Sample 2 in this configuration; one at an area on
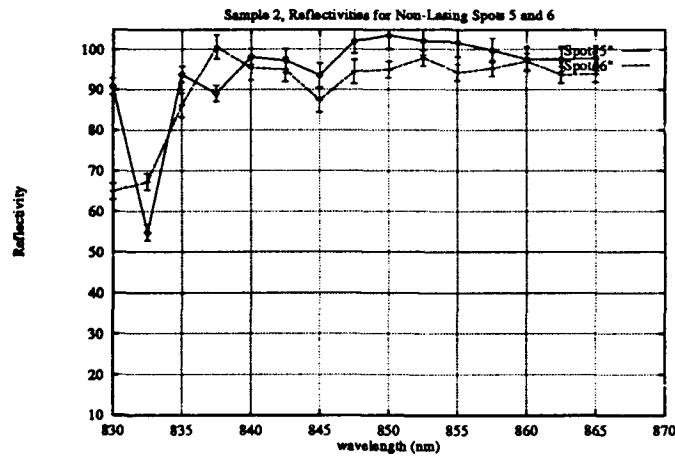
Figure 5.13.   Sample 2 Measured Spectral Reflectivity for Non-Lasing Locations: Spots 5 and 6

the wafer with many lasers, and another at an area with no lasers. This measurement was not possible for sample 1, which was much smaller than sample 2, and scattered much of the 3 mm pump spot. The reflectivities are contained in figure 5.14

5.3.3 **Sample 2 Analysis** The pump and lasing wavelengths for all four spots indicate higher wavelengths than predicted. The indications are that the actual lasing wavelength for the structure is nearer 885 nm than the designed 875 nm.

The reflectivity curves for spots 3 and 4 indicate a close match in reflectivities between adjacent lasing and non-lasing spots. The quality of the sample 2 wafer was appreciably better than sample 1, which was an earlier fabrication, has fewer mirror layers, and has been subjected to more handling. These and the non-oblique incidence spectral reflectivity curve indicate higher pump wavelengths than predicted for the structure. A plot of the non-oblique incidence measurements and a theoretical spectral reflectivity curve for an 887 nm GaAs VCSEL is shown in figure 5.15. The closer match is evident.

The non-oblique incidence (measurements with no focusing lens) spectral reflectivities indicate the non-lasing area has a significantly reduced reflectivity about the desired lasing wavelength. However, the reflectivities obtained with the focusing lens show that
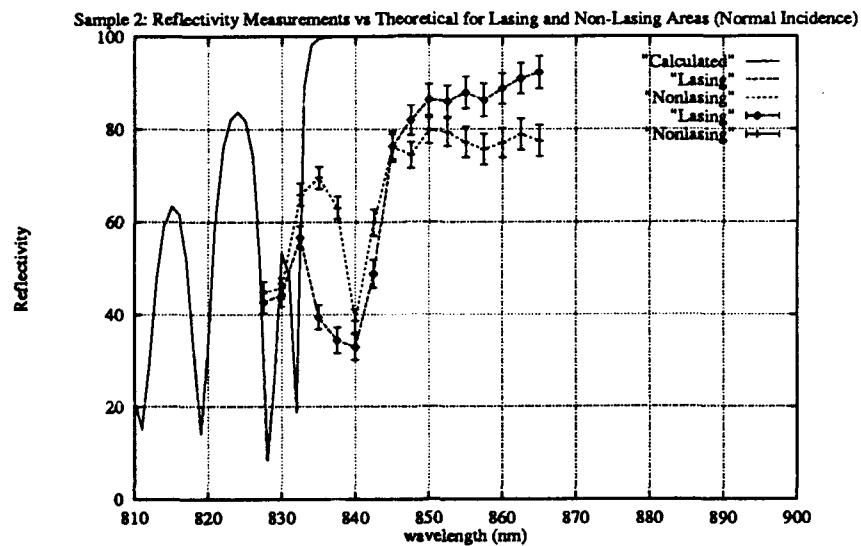
Figure 5.14.   Sample 2 Measured vs Theoretical (875 nm VCSEL) Spectral Reflectivities for Lasing and Non-Lasing Areas
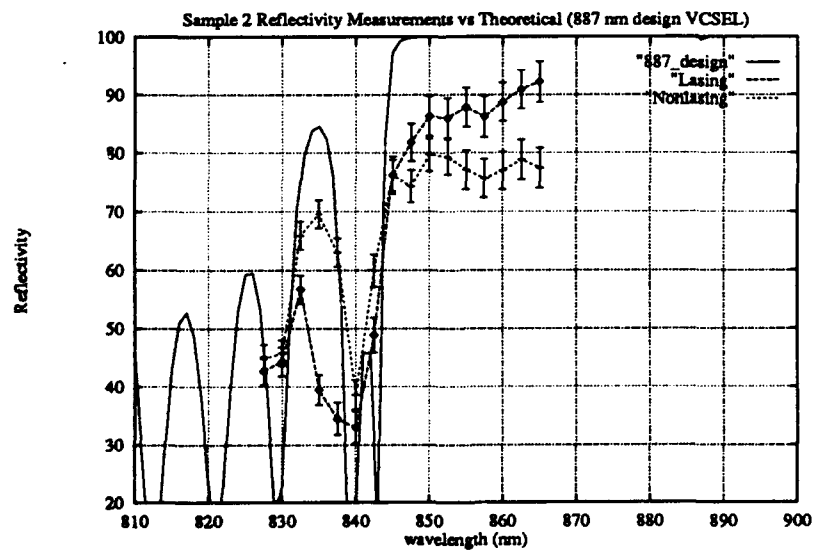
Figure 5.15.   Sample 2 Measured Spectral Reflectivities for Lasing and Non-Lasing Areas vs Theoretical (887 nm GaAs VCSEL)

reflectivities for adjacent lasing and nonlasing spots are nearly the same. Spectral reflectivity measurements, then, can give a general idea of the lasing prospects for the wafer, but do not guarantee a specific spot will lase.

All polarizations were linear and indicated a 90° rotation to those measured for sample 1. Again, no information regarding the growth direction was available, and it is likely this sample provides polarization orthogonal to that in sample 1 because the same physical mechanisms apply, but the sample is rotated 90° on the measurement stand.

As noted in the spot descriptions, both TEM_{10} and TEM_{00} modes were found on the sample. Pictures of these modes are provided in figure 5.9 and 5.11 above. The TEM_{10} lasing mode occurred on spot 3. The mode was stable, remaining unaltered for changes in pump intensity, wavelength, and position.

5.4 Design VCSEL Back Mirror

The initial back mirror was designed to measure the quality of the MBE fabrication before proceeding to the full VCSEL structure. The desired lasing wavelength and reflectivity between the GaAs spacer and the back mirror were the primary concern. The plot for the reflectivity in the GaAs spacer is in figure 3.4 on page 3-8. For experimental measurements, the back mirror reflectivity was to be determined with the incident medium being air, rather than GaAs. To stave off oxidation of the AlAs layers, a top $\lambda/4$ layer was deposited on the mirror stack, resulting a a 17 period stack of AlAs/GaAs pairs on a GaAs substrate.

5.4.1 Material Parameters The parameters for the bottom mirror in air were:

Number of Layers:	34
Substrate:	GaAs
Peak Reflectivity:	99.147 % @ 920 nm in air
Low Index Layers:	AlAs
Calculated Index @ 920 nm:	2.98151
Physical Layer width:	77.1 nm
High Index Layers:	GaAs
Calculated Index @ 920 nm:	3.5727
Physical Layer width:	64.3 nm
Wafer diameter:	50 mm

5.4.2 Back Mirror Measurements The spectral reflectivity curve in air for such a structure was computed and the curve is plotted in figure 5.17 along with the measured data for the grown wafer. The reflectivity attained by the wafer reaches the desired reflectivity for the bottom mirror. Since the calculated spectral reflectivity curves do not include absorption and scattering losses, the reflectivity obtained by the wafer, can't be expected to reach the predicted curve. The degree to which the shape of the measured spectral reflectivity curve matches the design curve indicates the proximity of the layer thicknesses to design thicknesses. The stop band width of the measured curve can indicate if the indices of refraction of the layers are close to those specified, as discussed in chapter II.

Initially, measurements were taken at two locations on the wafer; one set of data at the wafer center, and another at 10 mm radially out from the center. The configuration in figure 4.3 was used for these measurements, as that configuration, with the broad Ti-Sapphire wavelength range, provided a more complete spectral reflectivity measurement.

Wafer Center Spectral Reflectivity : The measurements shown in figure 5.16 were taken at a 7° oblique incidence, which shifts the spectral reflectivity curve to slightly shorter wavelengths than for normal incidence ($\approx$ 5 nm). The first minimum next to the stop band is very close to the desired wavelength, and the stop band width is nearly the same as predicted. This indicates the layer thicknesses and indices of refraction are as needed at the center of the wafer.
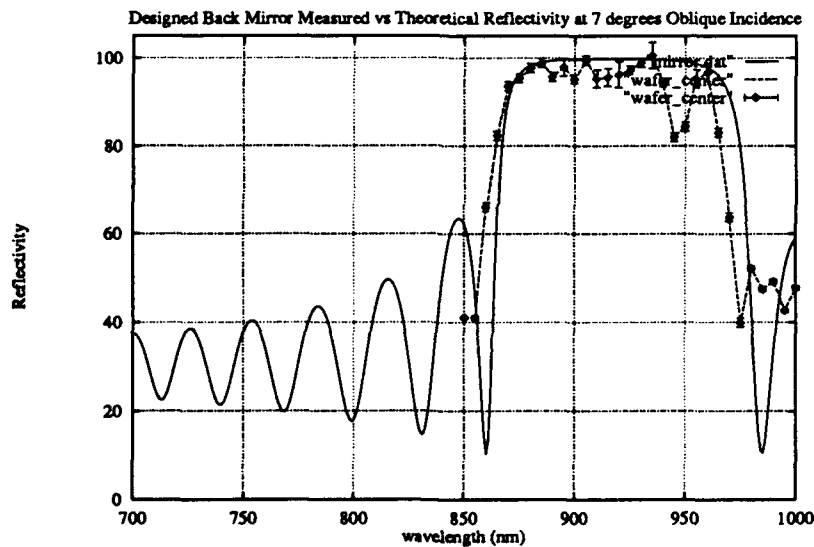
Figure 5.16. Spectral Reflectivity Measurements at Center of Designed 920 nm Back Mirror

Wafer 10 mm Spectral Reflectivity : The measurements at a location 10 mm out from the wafer center were taken at a 65° oblique incidence. This high angle of incidence shifts the spectral reflectivity curve ($\approx$ 28 nm) down. The spectral reflectivity curves here indicate a close match for the edge of the stop band and reproduce the secondary maximum at 970 nm well. No conclusions about the indices of refraction can be drawn,

since this curve has not captured both edges of the stop band, but it is unlikely the index for each layer will change with location on the wafer and the stop band in figure 5.16 indicates the designed refractive indices are present.
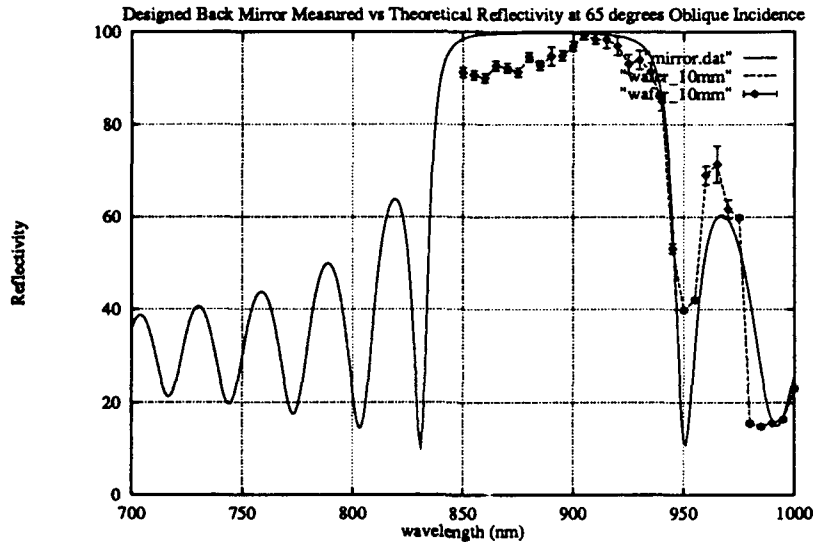
Figure 5.17.   Spectral Reflectivity Measurements at 10 mm radial out from Center of Designed 920 nm Back Mirror

Wafer Radial Measurement Comparisons : Comparison of reflectivities at locations on the wafer radially out from the center were next completed. Figure 5.18 contains a comparison of reflectivities for the center of the wafer, and for locations at 10 mm, and 20 mm radially out. Figure 5.19 is a comparison of two spots located 5 mm out from the center of the wafer. This is an indication of the uniformity of the growth at a constant radius.

Figure 5.18 shows a large variance in the reflectivity of the wafer as the spot is moved from the center of the wafer radially out to points 10 and 20 mm from center. The stop band tends to move to shorter wavelengths indicating the layers are becoming thinner. The high edge of the stop band near the edge (20 mm from center of wafer) has moved to 940 nm. This is approximately 35 nm from the calculated location of 40% reflectivity for a 7° oblique incidence (see *Calculated* curve in figure 5.16). If this shift is typical for this

5-20

radial, the Bragg frequency has moved to 885 nm, indicating the mirror layer thicknesses are reduced.
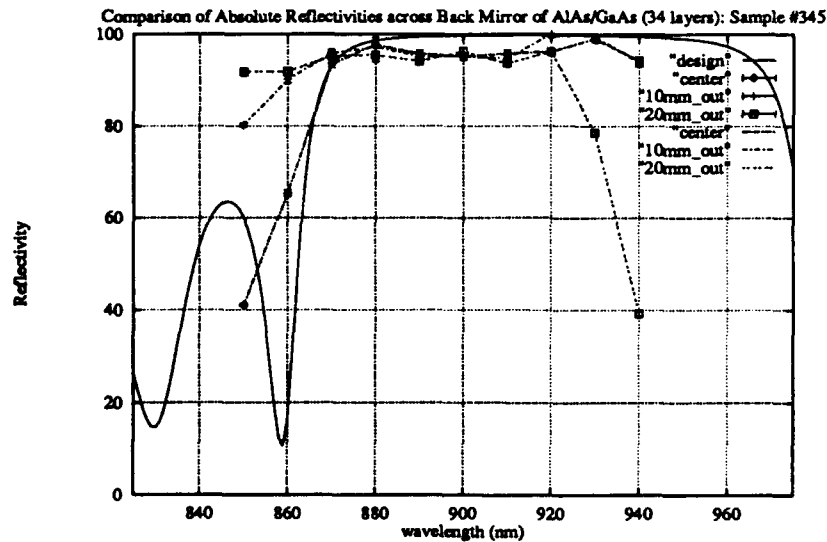
Figure 5.18. Spectral Reflectivity Measurements at Center, 10mm radial, and 20 mm radial of Designed 920 nm Back Mirror

To determine if the mirror layers were uniform on a constant radius from the center, two points on the wafer 5 mm from the center in opposing directions were measured. Uniform thickness on a constant radius is expected, since the wafer is rotated during the MBE growth specifically to improve this constant radius uniformity. The result of this measurement is shown in figure 5.19, and indicates the reflectivities for the two locations are very nearly the same. This radial uniformity can help to enlarge the areas of the wafer having the desired layer thicknesses
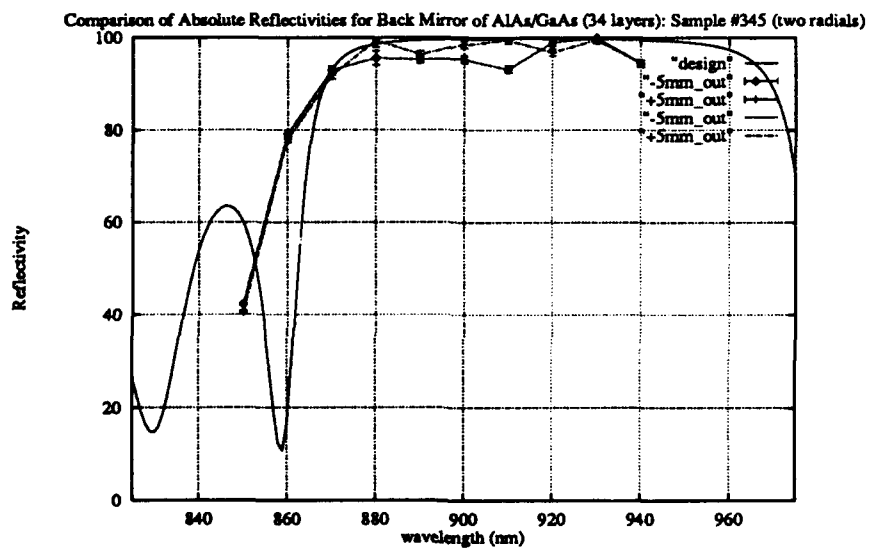
Figure 5.19. Spectral Reflectivity Measurements at two radials, 5mm from Center of Designed 920 nm Back Mirror

VI. Conclusion

The pace of improvements to the basic VCSEL design is continuously accelerating. This research verified the capability to locally produce VCSEL-quality structures and characterize their performance. The by-product of this effort is an initial in-house capability for design and characterization of VCSEL structures; and a nearby means for fabrication. The research purposely centered on optically pumped devices, due to the means of production available locally and the structures we could "borrow" from the University of Arizona.

6.1 Characterization

The laboratory configurations used for device characterization are detailed in chapter IV. The configuration in figure 4.1 provided the means to optically pump the VCSELs supplied by the University of Arizona, measure output beam characteristics, and measure spectral reflectivity from the wafer. The relatively narrow spectral range of the dye laser prompted additional measurements with the Ti-Sapphire system in figure 4.3. The Ti-Sapphire system provided a means to cover the entire stop band of the Fabry-Perot curve for the VCSELs.

Measurements were accomplished with and without a focusing lens. The lens was necessary to concentrate the pump on the VCSELs. The focusing lens also provided a means to isolate the reflectivity from an individual VCSEL structure. The convolving effect of the lens on the spectral reflectivity, however, was unwanted. Measurements without the focusing lens provided the spectral reflectivity for a broad area (3mm) relative to the VCSEL diameter ($\sim$ 3 - 20 μ m) without the convolving effect on the spectral reflectivity. These measurements, however, average the reflectivity of lasing and non-lasing spots on the wafer. Conclusions drawn and areas that warrant further investigation follow.

6.1.1 Spectral Reflectivity
Reflectivity measurements from lasing and non-lasing areas of the samples indicate a cursory spectral reflectivity measurement can quickly exclude samples with very poor reflectivity ($<$ 80 %). The measurements with focused pump spot show both lasing and non-lasing locations on the wafer can have nearly the same spectral

reflectivity. The reason why one area lases while an adjacent area does not should be investigated further. There may be multiple mechanisms at work.

Surface Roughness The scattering from the surface of the wafer may contribute to this effect, scattering more of the incident pump at the non-lasing location. One would expect a lower reflectivity from the area with more surface scatter, since not all the scattered light can be expected to reflect back toward the detector. Here, the action of the focusing lens (see figure 4.2) may act to collect a large part of the scattered light and provide no indication of how much of the light incident at the surface is actually entering the active region. When the pump intensity is increased, the scattering still results in a reduced pump intensity in the active region, possibly insufficient for the onset of lasing. A closer inspection of the surface roughness of the sample, with regard to lasing and non-lasing areas, would be in order. Future studies will need a precise, repeatable means of determining position on the wafer as the sample is moved from the lasing configuration to the microscopic analysis configuration to explore this phenomenon. The laboratory configuration in figure 4.1 provides precision and repeatability, but only if the sample is not moved from the positioner. This configuration does not lend itself to microscopic viewing of the sample.

Guide Mechanisms Another mechanism to explore is the gain/index guiding used to stimulate these optically pumped VCSELs. The use of injected carriers to self guide the lasing process may be affected by surface roughness also. Here, the pump input may be generating a sufficient amount of carriers in the active region, but the proximity of the active region to a more favorable exit spot may tend to channel the beam to that spot (see figure 6.1)

This prompts a reason for a phenomenon noted in the lab experiment. The imaged output of the laser spot tended to shift slightly ($\approx 1\mu m$) as the pump beam passed across the lasing location on the wafer. As the spot moved off the optical axis, the intensity decreased until lasing ceased, leaving a photoluminescent (but non-lasing) spot shifted back to the optical axis.
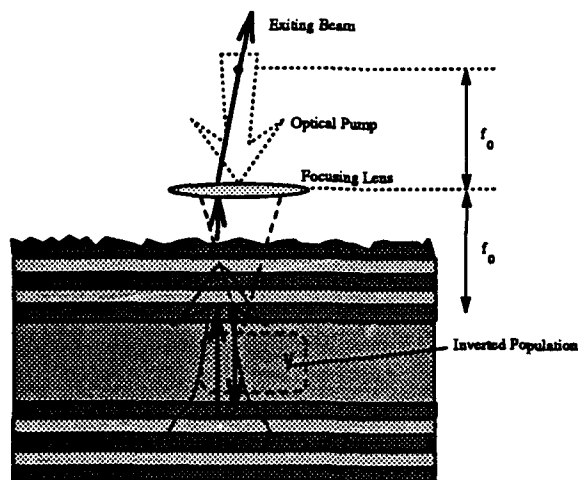
Figure 6.1. Non-Coincident Pump and Exit Beam Locations due to Surface Roughness

If surface roughness provides a more favorable exit point adjacent to the pump spot, the exiting beam would move to that location, feeding off the carriers generated at the pump location. With the lab configuration used for this effort, the focusing lens would image the exit beam at a point removed from the optical axis, as shown. The further the pump moves from this more favorable exit point, the more loss encountered by the carriers (they are on the fringes of the high gain region, and experience more loss), eventually, encountering too much loss to support lasing.

The ability to image larger areas on the wafer would enhance this study. The irregularities (especially the "islands" mentioned in chapter 5 in the spot 2 analysis) were approximately the same size as the pump spot, making it difficult to compare the irregularities to normal structures nearby. These "islands" were also witnessed in VCSEL imaging experiments at the University of Arizona [17], and, since they tend to exhibit lasing, may provide useful information for future growths.

6.1.2 **Polarization** With complete wafer growths available in the future, another possible avenue of investigation is the link of polarization and growth patterns. As discussed in chapter II the link between strained active regions and polarization has been established. The close lattice match of GaAs to the $Al_xGa_{1-x}As$ ternaries provides very

little strain. In his investigations, Jewell [21] found apparently random orientation to the linear polarization output beams from an optically pumped GaAs VCSEL. Further investigation into this area might show a link between polarization direction and growth patterns.

6.1.3 **Laboratory Configuration Improvements** Many of the improvements already planned will significantly improve the capability for characterization and VCSEL stimulation.

- -- The dye laser used in this experiment was difficult to maintain, had a limited frequency range, and exhibited output power fluctuations which made it difficult to capture reliable reflectivity data. The use of the Ti-Sapphire system highlighted these shortcomings. The seven measurements used in this report from the configuration with the Ti-Sapphire laser (see figure 4.3) were done in one day. The dye laser configuration would have taken at least five days to accomplish the same number of measurements and would not have been able to cover the desired frequency range.

- Faist [14] suggests transmission electron microscopy (TEM) is essential for more detailed analysis of the surfaces involved. Any future study into the surface roughness aspects of the problem will rely greatly on the availability of some form of microscopy for physical comparison to the lasing structure's behavior.

- The addition of an optical multichannel analyzer will significantly speed the spectral reflectivity measurements by using a broadband light source rather than a laser to perform these measurements.

6.2 **Design**

Design improvements can be accomplished in many areas. The vertical cavity structures described herein are intentionally entry level. Some immediate improvements in the efficiency of the VCSELs grown can be realized, some are longer term.

1. Incorporate separate confinement heterostructure (SCH) into the quantum well design described. This will improve the longitudinal confinement factor (Γ) for the active region, and would involve only a few extra growth layers.

2. Graded index (GRIN) quantum well structures to improve the capture of the carriers in the InGaAs wells.

3. Higher reflectivities in the mirrors should be attempted. Higher reflectivities will favor lower thresholds as long as the losses in the mirrors can be kept low. Coldren indicates the point of diminishing returns for three and two quantum well structures is near 99.7 % mean mirror reflectivity [9] and goes to lower reflectivities for more quantum wells.

4. The literature is very sparse on the material properties of $In_x Ga_{1-x}As$ on GaAs substrates. The lack of this data inhibits the ability of the designer to determine the cavity gain and loss profiles. Efficiency of the design depends on these parameters. Many of the major successes in the VCSEL efficiency and power areas have resulted from an in-house capability to measure prospective material parameters. Some suggest the construction of simpler in-plane lasers and subsequent parameter measurement in these devices to provide the necessary parameters for an efficient VCSEL design. This approach may be an appropriate measure if efficiency is to be pursued.

5. Ion implantation for gain guiding and etching for index guiding should be attempted. A comparison to an identically grown VCSEL wafer without etching or ion implantation could indicate if these processes provide an essential extra carrier confinement, and increase the number of usable lasers on the wafer.

6. The incorporation of electrical stimulation of the active medium, two dimensional arrays, coupled outputs, and visible wavelength structures make VCSEL fabrication an area with an extremely big potential return.

Appendix A. Spectral Reflectivity FORTRAN Programs

The programs below were first developed at the University of Arizona, and were modified to apply to the VCSEL structures and DBR mirrors measured for this thesis.

A.1 Program to Calculate the Spectral Reflectivity in Fabry-Perot Etalon with Distributed Bragg Reflector Mirrors (VCSEL Structure)

```
c program vcsel.f

c This program calculates the transmission and reflection of a GaAlAs
c Fabry-Perot etalon with integrated mirrors as a function of the input
c beam wavelength.

      PROGRAM vcsel

      real na,ns,lmbda1,lmbda2,lmb
      real lmbda,TRANS(1000),cosd(100),lmbda1,lmbda2
      real lmbdac, indxcL, indxcH, indxcs,indxH, indxL,indxs
      character*6, thick,oblique,pol,reflct,yorn,max
      complex indx(100),phase(100),cindxh,cindxl,cindxs
      complex r,t,s,u,rr,tt,ss,uu,rrr,ttt,sss,uuu,b,c
      common sina,lmbda

c         This section initializes the parameters for the menu,
c            allowing the star-up program to have a set of parameters
c            which will produce a default set of data.
c
      WRITE(*,2)
2       FORMAT(' ','The reflectivity data is in FP.dat')
        write(*,*) 'The current default parameters are:'
c            Number of front and back mirror layers
        NLF=22
        NLR=33
c          Spacer length
        spcerl=.515
c          Loss in the layers
        al=0.0
c          x concentrations in the low, high index layers and the spscer
        xl=1.0
        xh=0.0
        xs=0.0
c          Whether to allow changes in the layer thicknesses,
c             oblique incidence(which requires a polarization)
        thick='no'
        oblique='no'
        pol='TE'
c             Lasing wavelength
```

```
         lmbdac=.92
c              Beginning, ending, and spacing wavelength for plot
         lmbda1=.7
         lmbda2=1.
         nlmbda=300
c              Default layer Thickness variation factors, high index layers,
c              lowindex layers, and spacer
         fctorl=1.
         fctorh=1.
         fctors=1.
c            The incident medium for the reflection
         reflct='air'
c            Whether to remain in the program
         yorn='y'


c          This part of the program produces the menu on the screen

10       open(3, file='FP.dat')
         write(6,20) '[1] No. of layers front','[2] No. of layers back'
         write(6,25) NLF,NLR
20       FORMAT(10X,A, 10X, A)
25         FORMAT(14X,I, 16X, I)
         print*, ' '
         write(6,30) '[3]Al concentrations:','high n layer',
     &   'low n layer', 'spacer layer'
         write(6,35) xh,xl,xs
30       FORMAT(1X,A, 5X, A,5X,A,5x,A)
35         FORMAT(30X,f5.2, 12X, f5.2,11x,f5.2)
         print*, ' '

         write(6,40) '[4] Design Wavelength(nm)',
     &       '[5] Spacer Thickness '
         write(6,42) lmbdac*1000,spcerl
40         FORMAT(2X,A, 10X, A)
42         FORMAT(12X,f6.2, 30X, f6.3)
         write(*,*)
         write(6,45) '[6] Oblique Incidence',
     &       'Polarization '
         write(6,47) oblique, pol
45         FORMAT(2X,A, 15X, A)
47         FORMAT(12X,A, 27X, A)
         write(*,*)
         write(*,*)
         write(6,50) '[7] Plot Data in FP.dat','start (nm)',
     &   'end (nm)', 'number of points'
         write(6,55) lmbda1*1000,lmbda2*1000,nlmbda
50       FORMAT(1X,A, 5X, A,2X,A,2x,A)
55         FORMAT(29X,f7.1, 4X, f7.1,2x,I)
         write(*,*)
         write(*,*)
```

```
          write(6,60) '[8] Vary layer thickness'
          write(6,65) thick
60        FORMAT(1X,A)
65          FORMAT(10X,A)
          write(*,*)
          write(*,*)
          write(6,67) '[9] Absorption constant'
          write(6,68) al
67        FORMAT(1X,A)
68          FORMAT(10X,f6.2)
          write(*,*)
          write(*,*)
c
c             Here the interaction with the user starts, allowing changes
c              to parameters on the menu
c
          print*, 'Type in the parameter to change (one parameter
     &   at a time, 0 to proceed'
          read(*,*)choice
          if(choice.eq.1)then
            write(*,*) 'number of layers of the mirror=?'
            read(*,*) nlf
          endif
          if(choice.eq.2)then
            write(*,*) 'number of layers of the mirror=?'
            read(*,*) nlr
          endif
          if(choice.eq.3)then
            write(*,*) 'Al content of high-index layer=?'
            read(*,*) xh
            write(*,*) 'Al content of low-index layer=?'
            read(*,*) xl
              write(*,*) 'Al content of spacer'
              read(*,*) xa
          endif
          if(choice.eq.4)then
            write(*,*) 'design wavelength of mirror in nm=?'
            read(*,*) lmbdac
            lmbdac=lmbdac*.001
          endif
          if(choice.eq.5)then
            write(*,*) 'spacer thickness=?'
            read(*,*) spcerl
          endif
          if(choice.eq.6.and.oblique.eq.'no')then
            oblique='yes'
            write(*,*) 'Incidence angle in degrees?'
            read(*,*) angle
            write(*,*) 'Polarization, if TE, input 1:'
            read(*,*) npol
            if(npol.eq.0)then
```

A-3

```
          pol='TM'
         else
          pol='TE'
         endif
        elseif(choice.eq.6.and.oblique.eq.'yes')then
          oblique='no'
          angle=0.
          npol=1
          pol='TE'
        endif
        if(choice.eq.7)then
          write(*,*) 'lmbda1 (beginning wavelength: nm)'
          read(*,*) lmbda1
          lmbda1=lmbda1*.001
          write(*,*) 'lmbda1 (ending wavelength: nm)'
          read(*,*) lmbda2
          lmbda2=lmbda2*.001
          write(*,*) 'nlmbda (number of points)'
          read(*,*) nlmbda
        endif
        if(choice.eq.8.and.thick.eq.'no')then
          thick='yes'
          write(*,*) 'Thickness multiplier for High index layer=?'
          read(*,*) fctorh
          write(*,*) 'Thickness multiplier for Low index layer=?'
          read(*,*) fctorl
          write(*,*) 'Thickness multiplier for spacer=?'
          read(*,*) fctors
        elseif(choice.eq.8.and.thick.eq.'yes')then
          thick='no'
          fctorl=1.
          fctorh=1.
          fctors=1.
        endif
        if(choice.eq.9.and.reflct.eq.'cavity')then
          write(*,*) 'absorption constant=?'
          read(*,*) al
        endif

        if(choice.ne.0)goto 10
c
c       initializing constants for this run
c
      PI=3.141592
      angle=angle*PI/180.
      sina=sin(angle)
      na=1.
      conv=6.626e-34*3.e14/1.6e-19


c determine the width of high-index (indxH) layer (widthH) and
c low-index (indxL) layer (widthL). lamdac is the design frequency of
```

```
c the etalon.

      hvc=conv/lmbdac
      CALL REF(xl, hvc, indxcL)
      CALL REF(xh, hvc, indxcH)
      CALL REF(XS,HVC,INDXCS)
      SPCERL=SPCERL*FCTORS
      widthH = lmbdac/4./indxcH*FCTORH
      widthL = lmbdac/4./indxcL*FCTORL
        print*,'spacer index = ', indxcs
       WRITE(*,*) 'change mirror thickness? if yes, input 1'
      READ(*,*) number
      if(number.eq.1) then
      WRITE(*,*) 'THICKNESS of HIGH INDEX LAYER=?'
      READ(*,'(F5.3)') widthh
      WRITE(*,*) 'THICKNESS of LOW INDEX LAYER=?'
      READ(*,'(F5.3)') widthl
      endif

c        prints width of high, low and spacer layers for design
      write(*,111) widthh,widthl,SPCERL
 111     format(1x,'high in um=',f7.6,5x,'low=',f7.6,5x,'spacer=',f8.6)
      WRITE(4,75) WIDTHH,WIDTHL
      WRITE(4,80) INDXCH,INDXCL,INDXCS
 75   FORMAT(//,
     +1X,F5.3,5X,'HIGHINDX THCKNSS ',F6.4,/,'LOW INDX THCKNSS ',F6.4)
 80   FORMAT(//,'HIGH INDX INDEX ',F5.3,5X,'LOW INDX INDX ',F5.3,/,
     +'SPACER INDEX ',F5.3)
c calculate the transmission trans of the etalon as the wavelength is
c varied from lmbda1(um) to lmbda2(um).

      XX1=0.
      XX2=0.
      do 200 k=1,nlmbda+1

      lmbda=lmbda1+(lmbda2-lmbda1)/float(nlmbda)*float(K-1)
      lmb=lmbda*1000

c alphal is the absorption constant multiplied by the thickness.
          alphal=0.
          if( lmbda .lt. 0.875 ) alphal=al
          plmbda=lmbda/4/pi
          hv=conv/lmbda
          CALL REF(xl, hv, indxL)
          CALL REF(xh, hv, indxH)
          call ref(xs, hv, indxs)
          CALL REF(0.,HV,NS)
          xxx=-alphal*lmbda/4/pi
          cindxs=cmplx(indxs,xxx)
          xx1=xxx*0.
          cindxh=cmplx(indxh,xx1)
```

```
                cindxl=cmplx(indxl,0.)

c call the phase change phase(m) by passing thru each layer at
c wavelength lmbda.

                do 201 m = 2,nlf,2
                    indx(m) = cindxL
                    call pha(indx(m),widthL,cosd(m),phase(m))
201                 continue

                do 202 m = 1,nlf,2
                    indx(m) = cindxH
                    call pha(indx(m),widthH,cosd(m),phase(m))
202                 continue

                m=nlf+1
                indx(m)=cindxs
                call pha(indx(m),spcerl,cosd(m),phase(m))

                do 203 m = nlf+2,nlf+nlr+1,2
                    indx(m) = cindxL
                    call pha(indx(m),widthL,cosd(m),phase(m))
203                 continue

                do 204 m = nlf+3,nlf+nlr+1,2
                    indx(m) = cindxH
                    call pha(indx(m),widthH,cosd(m),phase(m))
204                 continue

c calculate the transmission trans at wavelength lmbda.
c refer to Thin-Film Optics (2/e) by A. Macleod.

                if(numbera.eq.1) then
                do 205 m=1,nlr+nlf+1
                if(npol.eq.1) indx(m)=indx(m)*cosd(m)
                if(npol.ne.1) indx(m)=indx(m)/cosd(m)
205                 continue
                endif

                r = ccos(phase(1))
                s = (0,1.) * csin(phase(1)) / indx(1)
                t = (0,1.) * csin(phase(1)) * indx(1)
                u = r

                do 206 m=2,nlr+nlf+1

                    rr = ccos(phase(m))
                    ss = (0,1.) * csin(phase(m)) / indx(m)
                    tt = (0,1.) * csin(phase(m)) * indx(m)
                    uu = rr
```

```
                    rrr = rr * r + tt * s
                    ttt = rr * t + tt * u
                    sss = ss * r + uu * s
                    uuu = uu * u + ss * t
                    r = rrr
                    t = ttt
                    s = sss
                    u = uuu
206                 continue

              b=r+s*ns
              c=t+u*ns

c facr is to include the effect by reflection at the substrate-air
c interface.
              FACR=1.-((NA-1)/(NA+1))**2
              trans(K)=4.*na*ns/cabs(na*b+c)**2*FACR
              REFL=cabs((na*b-c)/(na*b+c))**2

c lmbda is multiplied by 1000 to change the unit from um to nm.
c trans(k) and refl are multiplied by 100 to get % of transmission.
              WRITE(3,250) LMBDA*1000., REFL*100., trans(k)*100.

c the following is the routine to find peak positions and the
c corresponding peak values of transmission.
              IF(K.GT.1) XX1=TRANS(K)-TRANS(K-1)
              IF(XX2.GT.0.AND.XX1.L.0.) THEN
              WRITE(*,222) PEAK,tRANS(K-1)
              END IF
              XX2=XX1
              peak=LMBDA
200       continue
222   format(1x, 'peak position in um=',f8.6,3x,'transmission=',f8.6)
250     FORMAT(1X,3F10.5)
      CLOSE(3)
        write(*,*)
        write(*,*)
        print*,'continue?'
        read(*,*)yorn
        if(yorn.eq.'y')then
          goto 10
        endif
        END
c
c This subroutine calculates the phase change in passing thru
c each layer for given values of the refractive index ( xindx ), the
c thickness ( width ), the incident angle.
c
      subroutine pha(xindx,width,cosd,phase)
      complex xindx,phase
      common sina,xlmbda
```

```
            sinan=sina/real(xindx)
            asinan=asin(sinan)
            cosd=cos(asinan)
            phase = 2. * 3.141592 * xindx * width * cosd / xlmbda
            return
            end
c
c This subroutine calculates refractive index of AlGaAs for
c given values of Al composition ( xconc ) and wavelength ( ev, in
c units of eV).
c
            SUBROUTINE REF(Xconc, ev, XN)

            a0 = 6.3 + 19.0 * xconc
            b0 = 9.4 - 10.2 * xconc
            E0 = 1.425 + 1.155 * xconc + 0.37 * xconc * xconc
            E0D = 1.765 + 1.115 * xconc + 0.37 * xconc * xconc
            xki = ev / E0
            xkiso = ev / E0D
            fx = (2. - sqrt(1.+xki) - sqrt(abs(1.-xki))) / xki / xki
            fxso = (2. - sqrt(1.+xkiso) - sqrt(abs(1-xkiso))) / xkiso /xkiso
            val = E0 /E0D
            epis = a0 *( fx + 0.5 * val**1.5 * fxso) + b0
            xn = sqrt(epis)
            xx = 3.65 + (ev - 1.5)/.3 * .13
            if ((ev.ge.1.4.or.xx.lt.xn).and.xconc.eq.0.) xn = xx
            return
            end
```

A.2 Distributed Bragg Reflector Mirror Spectral Reflectivity Calculation Program

```
c This program calculates the reflection by a
c GaAlAs mirror as a function of the input beam wavelength.

            PROGRAM DBR
            integer nl,choice
            real nspace, nsub, lambda1, lambda2,top
            real lambda, TRANS(1000),cosd(100)
            real lambdac, indexcL, indexcH, indexH, indexL
            complex index(100),phase(100),cindexh,cindexl
            complex r,t,s,u,rr,tt,ss,uu,rrr,ttt,sss,uuu,b,c
            character*6, borf,thick,oblique,pol,reflct,yorn,max
            common sina,lambda

c         Setting menu defaults

c         Default choice of back mirror to be the calculated one
            borf='back'
```

```
c          Number of layers
          NL=33
c             x concentrations in the low, high index layers and the spacer
          xl=1.0
          xh=0.0
          xs=0.0
c          Whether to allow changes in the layer thicknesses,
c             oblique incidence(which requires a polarization)
          thick='no'
          oblique='no'
          pol='TE'
c          Lasing wavelength
          lambdac=.92
c          Beginning, ending, and spacing wavelength for plot
          lambda1=.7
          lambda2=1.
          nlambda=300
c
c             Default layer Thickness variation factors, high index layers,
c             lowindex layers, and spacer
          factorl=1.
          factorh=1.
c
c        Incident medium for the reflected light (cavity or air)
c         use cavity if you want the reflection the laser will experience
c            air if you want waht to expect when measured in the lab
          reflct='cavity'
c
c        Maximize reflectivity, will automatiacally throw out layers that
c           don't add reflectivity and notify you it did so
          max='yes'
          Stay in the program
          yorn='y'
c
c        This part of the program produces the menu on the screen
c
10        open(4, file='mirror.dat')
          write(6,20) '[1] Mirror','[2] No. of layers'
          write(6,25) borf,NL
20        FORMAT(10X,A, 10X, A)
25         FORMAT(14X,A, 11X, I)
          print*, ' '
          write(6,30) '[3]Al concentrations:','high n layer',
     &     'low n layer', 'spacer layer'
          write(6,35) xh,xl,xs
30        FORMAT(1X,A, 5X, A,5X,A,5x,A)
35         FORMAT(30X,f5.2, 12X, f5.2,11x,f5.2)
          print*, ' '

          write(6,40) '[4] Design Wavelength(nm)',
     &        '[5] Vary Layer Thickness '
```

```
        write(6,42) lambdac*1000,thick
40        FORMAT(2X,A, 10X, A)
42        FORMAT(12X,f6.2, 30X, A)
        write(*,*)
        write(6,45) '[6] Oblique Incidence (angle)',
     &      'Polarization '
        write(6,47) oblique,'(',angle,')', pol
45        FORMAT(2X,A, 15X, A)
47        FORMAT(12X,A,,2x,A,f5.1,A, 27X, A)
        write(*,*)
        write(*,*)
        write(6,50) '[7] Plot Data in mirror.dat','start (nm)',
     &      'end (nm)', 'number of points'
        write(6,55) lambda1*1000,lambda2*1000,nlambda
50        FORMAT(1X,A, 5X, A,2X,A,2x,A)
55        FORMAT(35X,f7.1, 4X, f7.1,2x,I)
        write(*,*)
        write(*,*)

        write(6,60) '[8] Reflectivity in the cavity or in air'
        write(6,65) reflct
60        FORMAT(1X,A)
65        FORMAT(10X,A)
        write(*,*)
        write(*,*)
        write(6,67) '[9] Maximize Reflectivity'
        write(6,68) max
67        FORMAT(1X,A)
68        FORMAT(10X,A)
        write(*,*)
        write(*;*)


c
c           Here the interaction with the user starts, allowing changes
c            to parameters on the menu
c

        print*, 'Type in the parameter to change (one parameter
     &    at a time, 0 to proceed'
        read(*,*)choice
        if(choice.eq.1.and.borf.eq.'back')then
          borf='front'
          nn=1
        elseif(choice.eq.1.and.borf.eq.'front')then
          borf='back  '
          nn=0
        endif
        if(choice.eq.2)then
          write(*,*) 'number of layers of the mirror=?'
          read(*,*) nl
        endif
```

```fortran
if(choice.eq.3)then
  write(*,*) 'Al content of high-index layer=?'
  read(*,*) xh
  write(*,*) 'Al content of low-index layer=?'
  read(*,*) xl
    write(*,*) 'Al content of spacer'
    read(*,*) xa
endif
if(choice.eq.4)then
  write(*,*) 'design wavelength of mirror in nm=?'
  read(*,*) lambdac
  lambdac=lambdac*.001
endif
if(choice.eq.5.and.thick.eq.'no')then
  thick='yes'
  write(*,*) 'Thickness multiplier for High index layer=?'
  read(*,*) factorh
  write(*,*) 'Thickness multiplier for Low index layer=?'
  read(*,*) factorl
elseif(choice.eq.5.and.thick.eq.'yes')then
  thick='no'
  factorl=1.
  factorh=1.
endif
if(choice.eq.6.and.oblique.eq.'no')then
  oblique='yes'
  write(*,*) 'Incidence angle in degrees?'
  read(*,*) angle
  write(*,*) 'Polarization, if TE, input 1:'
  read(*,*) npol
  if(npol.eq.0)then
   pol='TM'
  else
   pol='TE'
  endif
elseif(choice.eq.6.and.oblique.eq.'yes')then
  oblique='no'
  angle=0.
  npol=1
  pol='TE'
endif
print*, 'angle= ',angle
if(choice.eq.7)then
  write(*,*) 'lambda1 (beginning wavelength: nm)'
  read(*,*) lambda1
  lambda1=lambda1*.001
  write(*,*) 'lambda1 (ending wavelength: nm)'
  read(*,*) lambda2
  lambda2=lambda2*.001
  write(*,*) 'nlambda (number of points)'
  read(*,*) nlambda
```

```
        endif
        if(choice.eq.8.and.reflct.eq.'cavity')then
          reflct='air'
          nn=1
        elseif(choice.eq.8.and.reflct.eq.'air')then
          reflct='cavity'
          if(borf.eq.'back')nn=0
        endif
        if(choice.eq.9.and.max.eq.'yes')then
          max='no'
        elseif(choice.eq.9.and.max.eq.'no')then
          max='yes'
        endif

        if(choice.ne.0)goto 10
c
c        initializing constants for this run
c

        PI=3.141592
        angle=angle*PI/180.
        sina=sin(angle)
        conv=6.626e-34*3.e14/1.6e-19


c determine the width of high-index (indexH) layer (widthH) and low-index
c (indexL) layer (widthL). lamdac is the design frequency of the etalon.

        hvc=conv/lambdac
        CALL REF(xl, hvc, indexcL)
        CALL REF(xh, hvc, indexcH)

        top=xh
        nsub=3.6
        if(nn.eq.1)nsub=1.

c  To provide max reflectivity, we need to use the max index changes at
c  the substrate and spacer, or air interfaces
        if(max.eq.'yes')then
          if(mod(nl,2).eq.0.and.abs(nsub-indexcl).lt.abs
     &      (nsub-indexcH))then
            top=xl
            xl=xh
            xh=top
            print*,'Ending with high index to maximize reflection'
          elseif(mod(nl,2).eq.1.and.abs(nsub-indexcH).lt.abs
     &      (nsub-indexcL))then
            top=xl
            xl=xh
            xh=top
            print*,'Ending with low index to maximize reflection'
          endif
```

A-12

```
        write(*,*)
      if(top-xa.eq.0.)then
        print*, 'layer next to cavity adds no
&   reflectivity, discard?'
          read(*,*), yorn
          if(yorn.ne.'n')then
            nl=nl-1
            top=xl
            xl=xh
            xh=top
            print*,'number of layers is now: ', nl
            print*, 'layer next to cavity has x
&   concentration; ', xh
            write(*,*)
            write(*,*)
            endif
        endif
      endif


        CALL REF(xl, hvc, indexcL)
        CALL REF(xh, hvc, indexcH)
        if(nn.eq.0) call ref(0., hvc, nspace)
        widthH = lambdac/4./indexcH*FACTORH
        widthL = lambdac/4./indexcL*FACTORL

        if(xl.gt.xh)then
         print*, "widthH =", widthH, "  IndexcH = ", indexcH
         print*, "widthL =", widthL, "  IndexcL = ", indexcL
        else
         print*, "widthH =", widthl, "  IndexcH = ", indexcl
         print*, "widthL =", widthh, "  IndexcL = ", indexch
        endif
        write(*,*)
        write(*,*)

c calculate the transmissivity trans of the etalon as the wavelength is
c varied from lambda1(um) to lambda2(um).

        XX1=0.
        XX2=0.
        PP=0.

        do  k=1,nlambda+1
            lambda=lambda1+(lambda2-lambda1)/float(nlambda)*float(K-1)
            plambda=lambda/4/pi
            hv=conv/lambda
            CALL REF(xl, hv, indexL)
            CALL REF(xh, hv, indexH)
            call ref(xs, hv, nsub)
            call ref(xa, hv, nspace)
```

A-13

```
                    if(nn.eq.1)nsub=1.

                    cindexh=cmplx(indexh,-0.0)
                    cindexl=cmplx(indexl,-0.0)



                    do m = 2,nl,2
                            index(m) = cindexL
                            call pha(index(m),widthL,cosd(m),phase(m))
                    end do

                    do m = 1,nl,2
                            index(m) = cindexH
                            call pha(index(m),widthH,cosd(m),phase(m))
                    end do

c calculate the transmission trans at wavelength lambda.
c refer to Computer-aided Techniques for the Design of Multi-layer Filters
c (pp.9-10) by H.M. Liddell(1981, Adam Hilger).

                    if(numbera.eq.1) then
                    do m=1,nl
                    if(npol.eq.1) index(m)=index(m)*cosd(m)
                    if(npol ne.1) index(m)=index(m)/cosd(m)
                    end do
                    endif

                    r = ccos(phase(1))
                    s = (0,1.) * csin(phase(1)) / index(1)
                    t = (0,1.) * csin(phase(1)) * index(1)
                    u = r

                    do m=2,nl

                            rr = ccos(phase(m))
                            ss = (0,1.) * csin(phase(m)) / index(m)
                            tt = (0,1.) * csin(phase(m)) * index(m)
                            uu = rr

                            rrr = rr * r + tt * s
                            ttt = rr * t + tt * u
                            sss = ss * r + uu * s
                            uuu = uu * u + ss * t
                            r = rrr
                            t = ttt
                            s = sss
                            u = uuu
                    end do

                    b=r+s*nsub
```

A-14

```
            c=t+u*nsub
            trans(K)=4.*nspace*nsub/cabs(nspace*b+c)**2*100.
            REFL=cabs((nspace*b-c)/(nspace*b+c))**2*100.
            WRITE(4,70) LAMBDA*1000.,REFL, trans(k)

            if(LAMBDA+.001.ge.lambdac.and.lambda-.001.le.lambdac)then
            print*, "Wavelength: ", LAMBDA*1000, "  refl:  ", REFL
            endif
      end do
70    FORMAT(1X,3F10.5)
        close(4)
        write(*,*)
        write(*,*)
        print*,'continue?'
        read(*,*)yorn
        if(yorn.eq.'y')goto 10
        END


c
c This subroutine calculates the phase change in passing thru
c each layer for given values of the refractive index ( xindx ), the
c thickness ( width ), the incident angle.
c
        subroutine pha(xindex,width,cosd,phase)
         complex xindex,phase
         common sina,xlambda
         sinan=sina/real(xindex)
         asinan=asin(sinan)
         cosd=cos(asinan)
         phase = 2. * 3.141592 * xindex * width * cosd / xlambda
         return
         end


c
c This subroutine calculates refractive index of AlGaAs for
c given values of Al composition ( xconc ) and wavelength ( ev, in
c units of eV).
c
        SUBROUTINE REF(Xconc, ev, XN)

        a0 = 6.3 + 19.0 * xconc
        b0 = 9.4 - 10.2 * xconc
        E0 = 1.425 + 1.155 * xconc + 0.37 * xconc * xconc
        EOD = 1.765 + 1.115 * xconc + 0.37 * xconc * xconc
        xki = ev / E0
        xkiso = ev / EOD
        fx = (2. - sqrt(1.+xki) - sqrt(abs(1.-xki))) / xki / xki
        fxso = (2. - sqrt(1.+xkiso) - sqrt(abs(1-xkiso))) / xkiso / xkiso
        val = E0 /EOD
        epis = a0 *( fx + 0.5 * val**1.5 * fxso) + b0
        xn = sqrt(epis)
```

A-15

```
xx = 3.65 + (ev - 1.5)/.3 * .13
if ((ev.ge.1.4.or.xx.lt.xn).and.xconc.eq.0.) xn = xx
return
end
```

1. Adachi, S. "Material parameters of $In_{1-x}Ga_xAs_yP_{1-y}$ and related binaries," *Journal of Applied Physics*, *53*(12):8775–8792 (December 1982).

2. Adachi, S. "GaAs, AlAs, and $Al_xGa_{1-x}As$: material parameters for use in research and device applications," *Journal of Applied Physics*, *58*:R1 (August 1985).

3. Ahn, D. and S.L. Chuang. "Optical Gain and Gain Suppression of Quantum Well Lasers with Valence Band Mixing," *IEEE Journal of Quantum Electronics*, *QE-26*(13):13–24 (January 1990).

4. Babic, D. I. and S.W. Corzine. "Analytic Expression for the Reflection Delay, Penetration Depth, and Absorptance of Quarter-Wave Dielectric Mirrors," *IEEE Journal of Quantum Electronics*, *28*(2):514–524 (February 1992).

5. Brinkman, W.C. and P.A. Lee. "Coulomb effects on the gain spectrum of semiconductors," *Physical Review Letters*, *31*:237–240 (July 1973).

6. Burns, G.F. and C.G. Fonstadt. "Monolithics Fabrication of Strain-Free (Al,Ga)As Heterostructure Lasers on Silicon Substrate," *IEEE Photonics Technology Letters*, *4*(1):18–20 (January 1992).

7. Casey, H.C. and M.B. Panish. *Heterostructure Lasers: Part A, Fundamental Principles*. Quantum Electronics-Principles and Applications, Academic Press, New York, 1978.

8. Chang-Hasnain, C. J., et al. "Transverse mode characteristics of vertical cavity surface emitting lasers," *Applied Physics Letters*, *57*(3):218–220 (July 1990).

9. Coldren, L.Å., et al. "Efficient Vertical Cavity Lasers," *Optical and Quantum Electronics*, *24*:S105–S119 (1992).

10. Corzine, S.W. and L.A. Coldren. "Theoretical gain in compressive and tensile strained InGaAs/InGaAsP quantum wells," *Applied Physics Letters*, *59*(5):588–590 (July 1991).

11. Corzine, S.W., et al. "Design of Fabry-Perot Surface Emitting Lasers with a Periodic Gain Structure," *IEEE Journal of Quantum Electronics*, *25*(6):1513–1523 (June 1989).

12. Corzine, S.W., et al. "Theoretical Gain in strained InGaAs/AlGaAs quantum wells including valence band mixing effects," *Applied Physics Letters*, *57*(26):2835–2837 (December 1990).

13. Dutta, N.K. "Analysis of current spreading, carrier diffusion, and transverse mode guiding in surface emitting lasers," *Journal of Applied Physics*, *68*(5):1961–1964 (September 1990).

14. Faist, J., et al. "Characterization of $GaAs/(GaAs)_n(AlAs)_m$ Surface-Emitting Laser Structures through Reflectivity and High-Resolution Electron Microscopy Measurements," *Journal of Applied Physics*, *66*(3):1023–1032 (August 1989).

15. Fritz, I.J., et al. "Dependence of critical layer thickness on strain for $In_xGa_{1-x}As$ / GaAs strained layer superlattices," *Applied Physics Letters*, *46*:967–969 (May 1985).

16. Geels, R.S., et al. "Low Threshold Planarized Vertical Cavity Surface Emitting Lasers," *IEEE Photonics Technology Letters*, *2*(4):234–236 (April 1990).

17. Grantham, J. Instructor of Physics. Personal Interview. Air Force Institute of Technology, Wright-Patterson AFB OH, 1992.

18. Heavens, O.S. "Optical Properties of Thin Films," *Reports on Progress in Physics*, *23*(1) (1960).

19. Jewell, Jack L., et al. "Vertical-Cavity Surface-Emitting Lasers: Design, Growth, Fabrication, Characterization," *IEEE Journal of Quantum Electronics*, *27*(6):1332–46 (June 1991).

20. Jewell, J.L., et al. "Vertical cavity single quantum well laser," *Applied Physics Letters*, *55*(5):424–426 (July 1989).

21. Jewell, J.L., et al. "Lasing characteristics of GaAs microresonators," *Applied Physics Letters*, *54*(15):1400–1402 (April 1989).

22. Kolbas, R.M., et al. "Strained-Layer InGaAs-GaAs-AlGaAs Photopumped and Current Injection Lasers," *IEEE Journal of Quantum Electronics*, *QE-24*(8):1605–1613 (August 1988).

23. Koyama, F., et al. "1.5-1.6 μm GaInAsP/InP dynamic-single-mode (DSM) lasers with distributed Bragg reflector," *IEEE Journal of Quantum Electronics*, *QE-19*:1042–1051 (June 1983).

24. Landolt-Bornstein. *Numerical Data and Functional Relationships in Science and Technology*, *17a,22a*. Springer, Berlin, 1982.

25. Liddell, H.M. *Computer Aided Techniques for the Design of Multilayer Films*. Adam Hilger, Ltd, Bristol, 1981.

26. MacLeod, H.A. *Thin Film Optical Filters* (2 Edition). New York: MacMillan Publishing Company, 1986.

27. McIlroy, P., et al. "Analysis and Application of theoretical gain curves to the design of multiquantum-well lasers," *IEEE Journal of Quantum Electronics*, *QE-21*:1958–1963 (December 1985).

28. Pinkas, E, et al. "GaAs $Al_xGa_{1-x}As$ double heterostructure laser – Effects of doping on laser characteristics of GaAs," *Journal of Applied Physics*, *43*(6):2827–35 (June 1972).

29. Soda, H., et al. "GaInAsP/InP Surface Emitting Injection Lasers," *Japan Journal of Applied Physics*, *18*(12):2329 – 2330 (December 1979).

30. Sze, S.M. *Semiconductor Devices Physics and Technology*. John Wiley & Sons, 1985.

31. Tai, K., et al. "Drastic reduction of series resistance in doped semiconductor distributed Bragg reflector for surface emitting lasers," *Applied Physics Letters*, *56*(25):2496–2498 (June 1990).

32. Weisbuch, Claude and Borge Vinter. *Quantum Semiconductor Structures: Fundamentals and Applications.* Academic Press, Boston, 1991.

33. Yariv, A. *Optical Electronics* (4 Edition). CBS College Publishing, 1991.

Vita

Captain Richard J. Bagnell was born on 21 December, 1958 in Long Branch, N.J. He graduated from Raritan High School, Hazlet, N.J. in 1977. He received a Bachelor of Arts degree in Physics from the College of St. Thomas in St. Paul, Minnesota in 1982 on a Reserve Officers Training Corps scholarship. After commissioning, his first assignment was in the Air Force Institute of Technology's Undergraduate Engineering Conversion Program at the University of New Mexico. He graduated from UNM in 1984 with a Bachelor of Science degree in Electrical Engineering. Next assigned to the 6906th Electronic Security Squadron, Electronic Security Command, at Brooks AFB, TX, he was a project officer involved in planning, performing, and reporting on TEMPEST evaluations of Air Force mission critical equipments. TEMPEST is the unclassified term for the study of electromagnetic emanations from classified processing equipments. He then transferred to Hanscom AFB Massachusetts, where he led the test integration effort for the Space and Missile Warning System Program Office. Captain Bagnell entered AFIT in May of 1991.

Captain Bagnell is a member of the Eta Kappa Nu and Tau Beta Pi engineering Societies

Permanent address: 7 Amherst Lane
                        Hazlet, New Jersey 07730

December 1992   Master's Thesis

DESIGN AND CHARACTERIZATION OF OPTICALLY PUMPED VERTICAL CAVITY SURFACE EMITTING LASERS

Richard J. Bagnell

Air Force Institute of Technology, WPAFB OH 45433-6583

AFIT/GE/ENP/92D-01

Vertical Cavity Surface Emitting Lasers (VCSELs) are a form of semiconductor laser which have their cavity oriented orthogonally to the plane of the wafer. The orientation necessitates short cavities, highly reflective mirrors and a relatively high gain/loss ratio. Even so, the resultant superior exit beam characteristics and the tight packing density of the finished lasers provide strong motivation for pursuing the growth of these structures. This thesis details the design of an optically pumped InGaAs multiple quantum well periodic gain structure VCSEL with a 950 nm lasing wavelength. These growths were to be a first attempt at VCSEL construction, so part of this study included verification of the quality of the parts of the finished design. These measurements required the construction of a laboratory configuration to optically pump VCSELs and characterize them by spectral reflectivity, output beam polarization, mode, lasing wavelength, and optimal pump wavelength. Analysis of the characteristics for several VCSELs obtained from the University of Arizona, and the back mirror grown locally, illustrate the ability to use measured data and theoretical spectral reflectivity calculations to determine the quality of the growths.

Semiconductor Lasers, Gallium Arsenide Lasers, Semiconductor Devices, Surface Emitting Lasers, Distributed Bragg Reflector Stack, Vertical Cavity Structure, InGaAs Quantum Wells	115

SECURITY CLASSIFICATION OF REPORT	SECURITY CLASSIFICATION OF THIS PAGE	SECURITY CLASSIFICATION OF ABSTRACT	LIMITATION OF ABSTRACT
UNCLASSIFIED	UNCLASSIFIED	UNCLASSIFIED	UL